NATIONAL ADVISORY COMMITTEE FOR AERONAUTICS

TECHNICAL NOTE 3448

THEORETICAL ANALYSIS OF INCOMPRESSIBLE FLOW THROUGH A RADIAL-INLET CENTRIFUGAL IMPELLER AT VARIOUS WEIGHT FLOWS

I - SOLUTION BY A MATRIX METHOD AND COMPARISON WITH AN APPROXIMATE METHOD

By Vasily D. Prian, James J. Kramer, and Chung-Hua Wu

Lewis Flight Propulsion Laboratory
Cleveland, Ohio

Washington
June 1955

NATIONAL ADVISORY COMMITTEE FOR AERONAUTICS

TECHNICAL NOTE 3448

THEORETICAL ANALYSIS OF INCOMPRESSIBLE FLOW THROUGH A RADIAL-INLET CENTRIFUGAL IMPELLER AT VARIOUS WEIGHT FLOWS

I - SOLUTION BY A MATRIX METHOD AND COMPARISON WITH AN APPROXIMATE METHOD

By Vasily D. Prian, James J. Kramer, and Chung-Hua Wu

SUMMARY

A method for the solution of the incompressible, nonviscous flow through a centrifugal impeller, including the inlet region, is presented. Several numerical solutions are obtained for four weight flows through an impeller at one operating speed. The results are presented in a series of figures showing streamlines and relative velocity contours. A comparison is made with the results obtained by using a rapid approximate method of analysis.

INTRODUCTION

In order to provide the fundamental information about the internal flow necessary for the rational design of efficient centrifugal compressors, two-dimensional solutions of the potential flow through centrifugal compressors on both blade-to-blade and meridional surfaces have been obtained by means of relaxation methods in references 1 to 4. In addition, a three-dimensional potential-flow solution was obtained by similar means in reference 5. However, all these solutions are for impellers with inducer sections extended infinitely far upstream or to the axis of the impeller and thus yield no information concerning the flow behavior ahead of and at the entrance to blades of finite thickness or blades which are not alined with the inlet stream.

A rapid approximate method has been developed in reference 6 that will predict the blade surface velocities in centrifugal impellers. The accuracy of this method has been investigated for the region downstream of the inducer section. However, because of the lack of an exact solution of the flow in the inlet region, there has been no verification of the approximate method there.

Consequently, a method for analyzing the flow in a centrifugal impeller, including the inlet region, by numerical solution of the partial differential equation governing the flow was developed at the NACA Lewis laboratory and is presented herein. This method was applied to a 48-inch-diameter centrifugal impeller for both design and off-design flow conditions. The impeller is similar to that discussed in references 7 and 8. The results of the exact solution are compared with the results of the rapid approximate method of reference 6.

ANALYSIS

The formulation of the problem and the proposed method of solution of the problem are discussed in this section.

Statement of Problem

The basic assumptions which are made concerning the physical nature of the flow determine the partial differential equation governing the flow. The assigning of proper boundary conditions to the problem then determines the particular solution of the partial differential equation.

Assumptions. - The flow is assumed to be steady, incompressible, and nonviscous. The assumption of steady, nonviscous flow is customary in compressor flow analyses. Several solutions have been obtained taking compressibility into account (e.g., refs. 1 and 2). The addition of the condition of compressibility complicates the solution by a factor which was considered to be out of proportion with its value in this case. Therefore, the fluid was assumed incompressible.

The further assumption is made that the flow is constrained to a blade-to-blade surface of revolution which is symmetrical about the impeller axis. Although the flow is constrained to this surface, a variation in the thickness of the stream sheet provides a closer approximation to the actual case. The shape of the stream surface in the axial-radial plane as well as the thickness variation is defined as a function of radial position which is specified at the beginning of the solution.

The rear stagnation point is assumed to be located at the blade tip. The Kutta condition states that for a noncuspidate blade with a sharp trailing edge the rear stagnation point occurs at the tip. However, for an impeller with a rounded trailing edge the location of the rear stagnation point cannot be predicted. It was necessary, therefore, to assume the location of the rear stagnation point.

Differential equation. - In this analysis, the right-handed cylindrical coordinates r, θ, and z (see figs. 1 and 2) are used. All symbols are defined in the appendix. The angular velocity of the impeller

is denoted by ω and the fluid density by ρ. The stream-sheet thickness in the z-direction is represented by b. The trace of the stream surface in the axial-radial plane is given by specifying z as a function of r. The slope dr/dz of this curve is equal to the tangent of the angle between the axis of rotation and the tangent to the trace of the stream surface in the axial-radial plane and is denoted by λ (see fig. 2). Thus, the resultant velocity w is given by

$$w^2 = w_\theta^2 + w_r^2 \left(1 + \frac{1}{\lambda^2}\right)$$

where the subscripts r and θ indicate components in the r- and θ-directions, respectively.

The stream function Ψ is defined by the following differential equations:

$$\frac{\partial \Psi}{\partial r} = - b\rho w_\theta \tag{1a}$$

$$\frac{\partial \Psi}{\partial \theta} = rb\rho w_r \tag{1b}$$

In this report all derivatives with respect to r shall be understood to mean derivatives with respect to r on the stream surface, that is, $\partial/\partial r$ in this report shall correspond to the bold-faced $\partial/\partial r$ of reference 9, in which the differential equation for the type flow considered herein is derived. With these definitions and assumptions, the differential equation of the flow becomes (see ref. 9, p. 35)

$$\frac{\partial^2 \Psi}{\partial r^2} + \left(\frac{1}{r} - \frac{\partial \ln b}{\partial r}\right)\frac{\partial \Psi}{\partial r} + \frac{1}{r^2}\left(1 + \frac{1}{\lambda^2}\right)\frac{\partial^2 \Psi}{\partial \theta^2} = 2\omega b\rho \tag{2}$$

This equation, together with the boundary conditions, mathematically determines the problem.

Boundary conditions. - This analysis of the flow is a boundary-value problem of the first kind or a Dirichlet problem. Certain boundaries of the flow and the values of the stream function on these boundaries are specified. Furthermore, the flow is assumed to vary periodically in the circumferential direction, completing a cycle in one pitch angle, the angular distance between two adjacent blade mean lines. The rotational speed of the impeller and the weight flow through the compressor are also specified. The domain of the solution is extended sufficiently far upstream and downstream, so that the flow is assumed to be uniform at the upstream and downstream boundaries. With the addition of these conditions, the problem is determined mathematically.

Method of Solution

Superposition of four basic solutions. - The differential equation (eq. (2)) was solved by a superposition of four basic solutions. These four basic solutions form a set of linearly independent solutions such that all possible flows (including all tip speeds) are expressible as linear combinations of these basic solutions. The first of these, designated ψ_0, is a solution of equation (2) with the condition that no flow crosses the upstream and downstream boundaries and $\omega = \omega_0 \neq 0$.

The other three basic solutions, designated ψ_1, ψ_2, and ψ_3, are solutions of the linear homogeneous equation obtained by equating the left side of equation (2) to zero. Thus, if

$$L = \frac{\partial^2}{\partial r^2} + \left(\frac{1}{r} - \frac{\partial \ln b}{\partial r}\right)\frac{\partial}{\partial r} + \frac{1}{r^2}\left(1 + \frac{1}{\lambda^2}\right)\frac{\partial^2}{\partial \theta^2}$$

then ψ_1, ψ_2, and ψ_3 are solutions of

$$L(\psi) = 0$$

Because L is a linear operator, ψ_0 plus linear combinations of ψ_1, ψ_2, and ψ_3 will satisfy equation (2) for $\omega = \omega_0$.

Boundary conditions for four basic solutions. - The flow region is represented by abcdefgh in sketch (a).

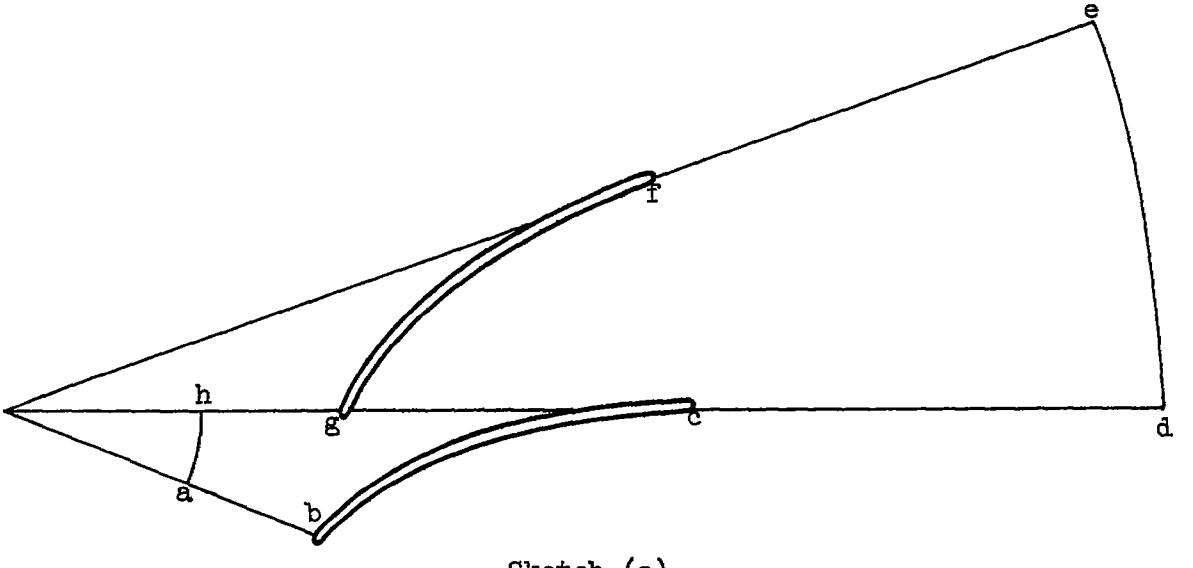

Sketch (a)

The upstream and downstream boundaries, ah and de, respectively, are placed sufficiently far from the blades so that flow conditions can be assumed uniform at these stations. The angular distance from a to h and from d to e is one pitch angle. For all the basic solutions, the condition that the flow is periodic about the axis of rotation with a period of one pitch angle makes it possible to obtain the solutions without a knowledge of the stream function along ab and gh. The finite-difference equation for points along these lines is obtained in the same manner as in reference 10. For the solution ψ_0 in which the flow is that induced only by the rotation of the impeller without any through flow, the value of ψ along ah and de is specified zero, indicating no flow crossing the upstream and downstream boundaries. The values along the blade surfaces bc and gf are also specified as zero. The solution to equation (2) for these boundary conditions is designated ψ_0.

The through-flow solution, that is, the flow through the stationary blade row, is obtained from linear combinations of three basic solutions to the homogeneous equation obtained by equating the left side of equation (2) to zero. All possible flows through the stationary blade row can be represented by linear combinations of these basic solutions. It can be seen from the boundary conditions shown in the following table that these three basic solutions are linearly independent.

Basic solution	Boundary values at			
	Point a	Point d	Point e	Point h
ψ_0	0	0	0	0
ψ_1	0	0	1	1
ψ_2	-1	0	1	0
ψ_3	-1	-1	0	0

The value of ψ along the trailing face is specified as zero and along the driving face as 1 for all three solutions. That these independent solutions are sufficient for the construction of all possible through flows can be seen from the following consideration.

Any flow is determined when the upstream and downstream flow conditions are specified. The velocity is assumed to be constant at stations ah and de. Hence, the stream function varies linearly from a to h and from d to e. Since the angular distance from a to h and from d to e is one pitch angle and the flow is assumed to vary periodically about the axis with a period of one pitch angle, the specification of conditions at points a, d, and h fixes the solution. The value of ψ is constant

along both the driving and trailing faces, with the difference between the function values being equal to $\psi_h - \psi_a$. The choice of 0 and ± 1 as the values of ψ at points a, h, d, and e and along bc and gf represents no restriction since these three basic solutions remain solutions to the homogeneous equation when changed by a multiplicative or additive constant.

Coefficients of ψ_0, ψ_1, ψ_2, and ψ_3 in linear combinations. - The final solution Ψ for any weight flow or rotational speed will be obtained from an equation of the form

$$\Psi = A_0\psi_0 + A_1\psi_1 + A_2\psi_2 + A_3\psi_3 \tag{3}$$

The coefficients A_0, A_1, A_2, and A_3 are determined by the specification of four independent physical conditions: (1) the rotational speed, (2) the weight flow, (3) the location of the rear stagnation point, and (4) irrotationality of the absolute flow.

The coefficient A_0 is determined by the rotational speed and is given by

$$A_0 = \frac{\omega}{\omega_0} \tag{4}$$

That is, A_0 is the ratio of the rotational speed ω for the desired solution to that used in obtaining the basic solution ω_0.

The change in Ψ across one blade passage is equal to the weight flow through a single passage. Therefore,

$$A_1 + A_2 + A_3 = M \tag{5}$$

where M is the weight flow through a single passage.

The rear stagnation point is assumed to be at the blade tip. Thus, at the tip,

$$w_\theta = 0$$

or

$$\left(\frac{\partial \Psi}{\partial r}\right)_t = 0 \tag{6}$$

This derivative is expressed in finite-difference form for the grid point at the blade tip and with equation (3) yields a linear relation in A_0, A_1, A_2, and A_3.

The absolute flow is irrotational, so that, if r_1 and r_2 are radial stations upstream of the blade row, the following equation holds:

$$\int_0^{2\pi} (w_{\theta,2} + \omega r_2) r_2 d\theta - \int_0^{2\pi} (w_{\theta,1} + \omega r_1) r_1 d\theta = 0 \tag{7}$$

where the subscripts 1 and 2 indicate values along the lines $r = r_1$ and $r = r_2$, respectively. If r_1 is chosen equal to the value of r at the upstream boundary, equation (7) becomes

$$\int_0^{2\pi} r_2 w_{\theta,2} \, d\theta = -2\omega\pi r_2^2 \tag{8}$$

since $w_{\theta,1}$ is equal to $-\omega r_1$. When the stream-function definition (eq. (1a)) is introduced, equation (8) becomes

$$\int_0^{2\pi} \frac{\partial \Psi}{\partial r} \, d\theta = 2\pi\omega\rho b_2 r_2 \tag{9}$$

Equation (9) can be integrated numerically to yield a linear relation in A_0, A_1, A_2, and A_3.

Equations (4), (5), (6), and (9) form a system of four simultaneous independent equations in four unknowns A_0, A_1, A_2, and A_3.

Numerical method of obtaining basic solutions. - The region of solution was covered with a network of grid lines whose intersections form grid or nodal points, as shown in figure 1.

The solution for a given set of boundary conditions of the differential equation was obtained at each of these grid points by solving the set of linear simultaneous equations obtained when the differential equation is written in finite-difference form for each grid point. A five-point system was used in the finite-difference approximation of the derivatives. This procedure is equivalent to approximating the stream function by a fourth-degree polynomial in the neighborhood of the grid point. The

solution of the set of n linear simultaneous equations was obtained on high-speed digital computers by the matrix method outlined in reference 10. Since there were four basic solutions, four sets of n simultaneous linear equations were solved by this process.

Numerical Example

The previously outlined method was applied in order to analyze the flow in a 48-inch-diameter radial-inlet centrifugal impeller. A description of the geometry of the impeller and the operating conditions for which the analysis was carried out follows.

Geometry of impeller. - The impeller investigated was a 48-inch-tip-diameter radial-inlet centrifugal impeller having 18 blades, similar to that discussed in references 7 and 8. The sharp leading edge and blunt trailing edge were rounded as shown in figure 1 because of practical computing considerations. The blade coordinates are given in table I. The solution was obtained on the surface generated by rotating the mean blade-height line about the axis of rotation. This line was approximated by the following function:

$$z = \frac{-0.041456}{(r - 0.40828)} + \text{constant} \tag{10}$$

The streamline spacing in the axial-radial plane is not known. Therefore, the stream-sheet thickness b in the z-direction was approximated by the blade height in the z-direction. This parameter was approximated by the following function:

$$b = 0.07208 + 1.01517\ e^{-1.54601r} \tag{11}$$

The parameter λ is equal to dr/dz of the stream-surface trace in the axial-radial plane and from equation (10) is given by

$$\frac{1}{\lambda} = \frac{0.041456}{(r - 0.40828)^2} \tag{12}$$

Operating conditions. - Four solutions were obtained corresponding to four weight flows at a tip speed of 700 feet per second. These four weight flows, which correspond to those of reference 9, are shown in the following table:

Case	Weight flow, lb/sec
A	14
B	26.25
C	32.10
D	44

RESULTS AND DISCUSSION

The results of the solutions obtained by the application of the previously outlined method are presented in figures 3 and 4, which show streamlines and constant relative velocity contours, respectively. Figures 3 and 4 are projections on the $r\theta$-plane, that is, the curvature of the stream surface in the axial-radial plane is neglected. The comparison with the results of the approximate method described in reference 6 is made in figure 5.

It was considered desirable to obtain the distribution of the velocity at the blade nose in more detail than was obtained by this solution. Therefore, a refinement of the solution in this region was made by relaxation methods and is presented in reference 11.

Streamlines

The distribution of stream function is shown by means of contours of constant stream-function ratio Ψ/M in figure 3 for the four weight flows investigated. The impeller tip speed was 700 feet per second for all four cases.

Case A. - In figure 3(a) the streamlines for a weight flow of 14 pounds per second are shown. This condition is the incipient surge weight flow for the experimental case (ref. 9). A large eddy attached to the driving face of the blade extends from $r \sim 1.30$ to $r \sim 1.84$ and almost one-third the distance across the passage between blades at its widest point. A stagnation point exists near the center of this eddy region. The major part of the flow is concentrated in the region near the trailing face, while the eddy and other relatively low-momentum fluid occupy half the channel.

After the flow is turned to the blade direction in the inlet region, the flow outside the eddy remains roughly parallel to the trailing face of the blade to $r \sim 1.5$. Slip then begins to occur and the slip factor, the ratio of the mass-averaged absolute tangential velocity of the fluid at the tip to the absolute tip speed, is equal to 0.874.

Case B. - The streamline pattern for the experimental peak pressure ratio and peak-efficiency weight flow (26.25 lb/sec) is shown in figure 3(b). This weight flow is sufficiently high to eliminate the eddy on the driving face of the blade. However, a fairly large concentration of low-momentum air is still present, so that halfway through the impeller 50 percent of the fluid occupies more than two-thirds the available flow area. Slip begins at $r \sim 1.50$, and the slip factor is 0.873.

Case C. - The streamline pattern for a weight flow of 32.10 pounds per second (fig. 3(c)) is similar to that for 26.25 pounds per second because of the comparatively small change in weight flow. The flow continues to shift toward the driving face, and the slip factor is 0.871.

Case D. - In figure 3(d), the streamline pattern is shown for a weight flow of 44 pounds per second. In the investigation reported in reference 7 this represented the maximum weight flow. The flow is distributed across the passage more nearly uniformly than in the other examples. The flow ceased to be perfectly guided at $r \sim 1.50$, as occurred for all other weight flows. The slip factor for this condition is 0.859, so that the total variation in slip factor from surge to maximum weight flow is only 0.015.

Relative Velocity

As stated previously, the solution in the immediate neighborhood of the nose was refined and is reported in reference 11. Hence, no discussion of the nose region is presented herein.

Case A. - Contours of constant relative velocity ratio W (relative velocity divided by tip speed) are plotted in figure 4(a) for a weight flow of 14 pounds per second. Downstream of the leading edge along the trailing face, there is a deceleration up to $r \sim 1.2$. The velocity then remains constant to $r \sim 1.70$, where a deceleration begins and continues to the stagnation point at the tip. Along the driving face, the flow decelerates after the slight acceleration just downstream of the stagnation point. This deceleration continues to the stagnation point at $r \sim 1.30$, at which point the eddy begins to form. The eddy exists along the greater part of the blade. There is a slight acceleration near the tip.

Case B. - In figure 4(b) the velocity contours for a weight flow of 26.25 pounds per second are shown. After the slight deceleration just downstream of the leading edge, the velocity along the trailing face is constant (except for a small acceleration and deceleration at $r \sim 1.3$) to $r \sim 1.70$. The flow then decelerates to the stagnation point at the tip. Along the driving face, the velocity decreases to $r \sim 1.36$ and then is constant to $r \sim 1.80$. The flow begins to accelerate and then decelerates to the tip stagnation point.

Case C. - Figure 4(c) presents the velocity contours for a weight flow of 32.10 pounds per second. The velocity along the trailing face is constant from $r \sim 1.0$ to $r \sim 1.3$ after the deceleration just downstream of the leading edge. At $r \sim 1.3$, a slight acceleration followed by a rapid deceleration occurs. This velocity peak is caused by the beginning of more rapid blade curvature at that point. This effect of the blade curvature is more evident for the higher weight flows than for the lower

because of the absence of the deceleration on the trailing face just downstream of the leading edge for the higher weight flows. Downstream of this rapid deceleration caused by the blade curvature, the velocity is constant from $r \sim 1.35$ to $r \sim 1.7$. The usual deceleration to the stagnation point begins at that point. On the driving face, the flow decelerates from just downstream of the leading edge to $r \sim 1.4$. The velocity is then constant to $r \sim 1.7$ where the flow begins to accelerate slightly, followed by the deceleration to the stagnation point.

Case D. - The velocity contours for a weight flow of 44 pounds per second are plotted in figure 4(d). The flow along the driving and trailing faces is similar to that for 32.10 pounds per second, because in both cases the inlet flow is directed toward the trailing face. The local acceleration and deceleration on the trailing face at $r \sim 1.3$ is more pronounced.

Angle of attack. - The approximate mean angle of attack, that is, the angle between the mean flow direction at the inlet and the tangent to the blade mean line, was computed from the rotational speed and the average inlet velocity. The average inlet velocity was computed from the weight flow and the annular area. Two values were used for the annular area: (1) the total annular area with no blade blockage assumed, and (2) the total annular area minus the blockage caused by the blades. The thickness of the blades used in the latter computation was that at the 1.4-foot radius, which was approximately the radius at which maximum blade thickness in the tangential direction occurred. The mean angle of attack across the passage at the 1.4-foot radius was also computed from the exact solution. These are compared in the following table:

Weight flow, lb/sec	Angle of attack, based on -		
	Unblocked annulus, deg	Blocked annulus, deg	Exact solution, deg
14	12.3	9.2	0
26.25	.1	-4.6	-5.3
32.10	-4.9	-10.0	-9.0
44	-13.6	-19.0	-15.4

The sign convention for the angle of attack is such that a positive angle of attack indicates flow directed towards the driving face of the blade. From the comparison of these angles of attack, it is apparent that the mean angle of attack is best predicted by basing the calculations on the annular area with blade blockage considered. The poor agreement between the mean angle of attack of the exact solution and that based on the blocked-inlet annular area at the lowest weight flow is probably caused by the eddy. It also appears from these average angles of attack that the original blade shape shown by the dashed line in figure 1 would perform better at a weight flow of 26.25 pounds per second. The blade angle

of the driving face just downstream of the rounded leading edge is 57°, whereas the angle between the mean line and the radial direction is 62°. Thus, at the weight flow of 26.25 pounds per second the average inlet flow angle would approximately equal the driving-face blade angle.

Comparison with Approximate Method

The blade surface velocities for the four weight flows were computed by the rapid approximate method of reference 6 in order to determine the accuracy of the approximate method, especially in the inlet region, by comparison with the matrix solution. In figure 5, the surface velocity ratios as computed by the approximate method are compared with the surface velocity ratios as determined by the matrix method. The velocity ratios are plotted against distance s along the blade mean line.

In the approximate method the mass-averaged velocity ratio W_m is assumed equal to the average of the blade surface velocity ratios W_{av}. The mass-averaged flow angle β_m is assumed equal to the average of the blade surface angles β_{av} for values of $s \leq 1.34$. For $s > 1.34$, β_m is approximated by a parabolic variation (with r) between the average of the blade surface angles at $s = 1.34$ and the flow angle at the tip as determined by the slip factor. The slope $d\beta_{av}/dr$ at $s = 1.34$ is used as the third condition to determine the parabola. The approximate flow angle as given by the parabolic variation is also denoted by β_{av}. In order to evaluate the validity of these assumptions, β_m is compared with β_{av} and W_m is compared with W_{av} in figures 6 and 7, respectively.

It was impossible to obtain meaningful results in the region of the rounded leading edge. This failure of the approximate method is caused by the invalidity of the assumption that β_m is equal to β_{av}. For values of s such that $0.07 \leq s \leq 0.6$, the surface velocities are predicted adequately for cases B and C but poorly for cases A and D. For case A the failure is probably caused by the change in the relative size of β_{av} and β_m. At $s = 0.6$, β_{av} is greater than β_m but then becomes less than β_m as s decreases. This trend is not followed in the other cases. For case D the agreement of W_{av} with W_m and of β_{av} with β_m is poorer for $s < 0.6$ than for the other cases. The trends for case D, however, were the same as for cases B and C.

In the region $0.6 \leq s \leq 1.8$, the agreement between the approximate solution and the exact solution is adequate (except in the neighborhood of $s = 0.8$ for cases B, C, and D) for approximately predicting both the velocity and the velocity gradients for all four weight flows. Such good agreement is surprising for case A because the agreement between

W_m and W_{av} and between β_m and β_{av} is not nearly so good for case A as it is for the other cases; the eddy attached to the driving face for case A is the cause of this poor agreement.

For $s > 1.8$, the agreement between the approximate method and the exact method is poor and β_{av} is less than β_m for all four cases except near the tip in case A. This reverse in trend, together with the fact that the blade surface angles differ by a large amount, probably is the reason for the failure of the approximate method near the tip. In the region $s > 1.34$, β_{av} is determined by a parabolic approximation to β_m. Since β_{av} and β_m agree fairly well at $s = 1.34$ and at the tip, the failure of the parabolic approximation must be attributed to incorrect values of $d\beta_{av}/dr$ at $s = 1.34$ or to the inadequacy of a parabolic approximation.

SUMMARY OF RESULTS

A method for the solution of the incompressible nonviscous flow through a centrifugal impeller (including the inlet region) is presented and is applied to a 48-inch-diameter centrifugal impeller. Solutions were obtained for four weight flows ranging from incipient surge to maximum as determined by actual impeller tests. The blade surface velocities obtained by these solutions were compared with those obtained by a rapid approximate method of analysis. The following results were noted:

1. A large eddy formed on the driving face of the blade at the incipient surge weight flow but was not present for the three higher weight flows.

2. The slip factor varied from 0.874 to 0.859 as the weight flow increased.

3. For weight flows of 26.25, 32.10, and 44 pounds per second, a local acceleration followed by a rapid deceleration occurred on the trailing face of the blades at a radius of about 1.3 feet, that is, where the blade begins to curve more rapidly.

4. The rapid approximate method was adequate in the inlet region just downstream of the leading edge for weight flows of 26.25 and 32.10 pounds per second. These weight flows corresponded to mean angles of attack of -5.3° and -9.0°, respectively.

5. The mean angle of attack was best predicted by basing the approximate computation on the weight flow, the tip speed, and the annular area minus the blockage of the blades.

Lewis Flight Propulsion Laboratory
National Advisory Committee for Aeronautics
Cleveland, Ohio, March 4, 1955

APPENDIX - SYMBOLS

The following symbols are used in this report:

A_0, A_1, A_2, A_3	coefficients in eq. (4)
b	stream-sheet thickness in z-direction, ft
M	weight flow through single passage, lb/sec
r	radial distance, ft
s	distance along blade mean line, ft
W	ratio of relative velocity to tip speed
w	relative velocity, ft/sec
z	axial distance, ft
θ	angular coordinate in relative system, radians
λ	slope of trace of stream surface in axial-radial plane
ρ	fluid density, lb/cu ft
Ψ	stream function, eq. (1)
$\psi_0, \psi_1, \psi_2, \psi_3$	basic solutions
ω	angular velocity of impeller, radian/sec

Subscripts:

av	approximation to mass-averaged value used in approximate method
m	mass-averaged value
r	component in radial direction
t	impeller tip
θ	component in tangential direction
0	value in basic solution of eq. (2)
1,2	conditions along $r = r_1$ and $r = r_2$, respectively

REFERENCES

1. Stanitz, John D., and Ellis, Gaylord O.: Two-Dimensional Compressible Flow in Centrifugal Compressors with Straight Blades. NACA Rep. 954, 1950. (Supersedes NACA TN 1932.)

2. Ellis, Gaylord O., and Stanitz, John D.: Two-Dimensional Compressible Flow in Centrifugal Compressors with Logarithmic-Spiral Blades. NACA TN 2255, 1951.

3. Ellis, Gaylord O., Stanitz, John D., and Sheldrake, Leonard J.: Two Axial-Symmetry Solutions for Incompressible Flow Through a Centrifugal Compressor with and without Inducer Vanes. NACA TN 2464, 1951.

4. Stanitz, John D., and Ellis, Gaylord O.: Two-Dimensional Flow on General Surfaces of Revolution in Turbomachines. NACA TN 2654, 1952.

5. Ellis, Gaylord O., and Stanitz, John D.: Comparison of Two- and Three-Dimensional Potential-Flow Solutions in a Rotating Impeller Passage. NACA TN 2806, 1952.

6. Stanitz, John D., and Prian, Vasily D.: A Rapid Approximate Method for Determining Velocity Distribution on Impeller Blades of Centrifugal Compressors. NACA TN 2421, 1951.

7. Michel, Donald J., Ginsburg, Ambrose, and Mizisin, John: Experimental Investigation of Flow in the Rotating Passages of a 48-Inch Impeller at Low Tip Speeds. NACA RM E51D20, 1951.

8. Prian, Vasily D., and Michel, Donald J.: An Analysis of Flow in Rotating Passage of Large Radial-Inlet Centrifugal Compressor at Tip Speeds of 700 Feet Per Second. NACA TN 2584, 1951.

9. Wu, Chung-Hua: A General Theory of Three-Dimensional Flow in Subsonic and Supersonic Turbomachines of Axial-, Radial-, and Mixed-Flow Types. NACA TN 2604, 1952.

10. Wu, Chung-Hua, and Brown, Curtis A.: A Theory of the Direct and Inverse Problems of Compressible Flow Past Cascade of Arbitrary Airfoils. Jour. Aero. Sci., vol. 19, no. 3, Mar. 1952, pp. 183-196.

11. Kramer, James J.: Theoretical Analysis of Incompressible Flow Through a Radial-Inlet Centrifugal Impeller at Various Weight Flows. II - Solution in Leading-Edge Region by Relaxation Methods. NACA TN 3449, 1955.

TABLE I. - MODIFIED BLADE COORDINATES

Driving face		Trailing face	
r	θ	r	θ
1.0405	0.73321	1.0285	0.72685
1.0521	.72685	1.0352	.69779
1.0696	.70353	1.0405	.68973
1.0740	.69780	1.0518	.66871
1.1190	.63965	1.0696	.64304
1.1278	.62944	1.0971	.61056
1.1711	.58150	1.1278	.57638
1.2324	.52335	1.1511	.55241
1.2441	.51335	1.2144	.49426
1.3095	.46520	1.2441	.47164
1.3604	.43582	1.2974	.43611
1.4262	.40705	1.3525	.40704
1.4767	.39101	1.3604	.40350
1.5930	.36851	1.4283	.37798
1.7093	.36080	1.4767	.36464
1.8256	.35976	1.5600	.34890
1.9419	.35976	1.5930	.34536
2.0000	.35497	1.7093	.33994
2.0123	.34890	1.8256	.34161
		1.9419	.34265
		2.0000	.34432
		2.0123	.34890

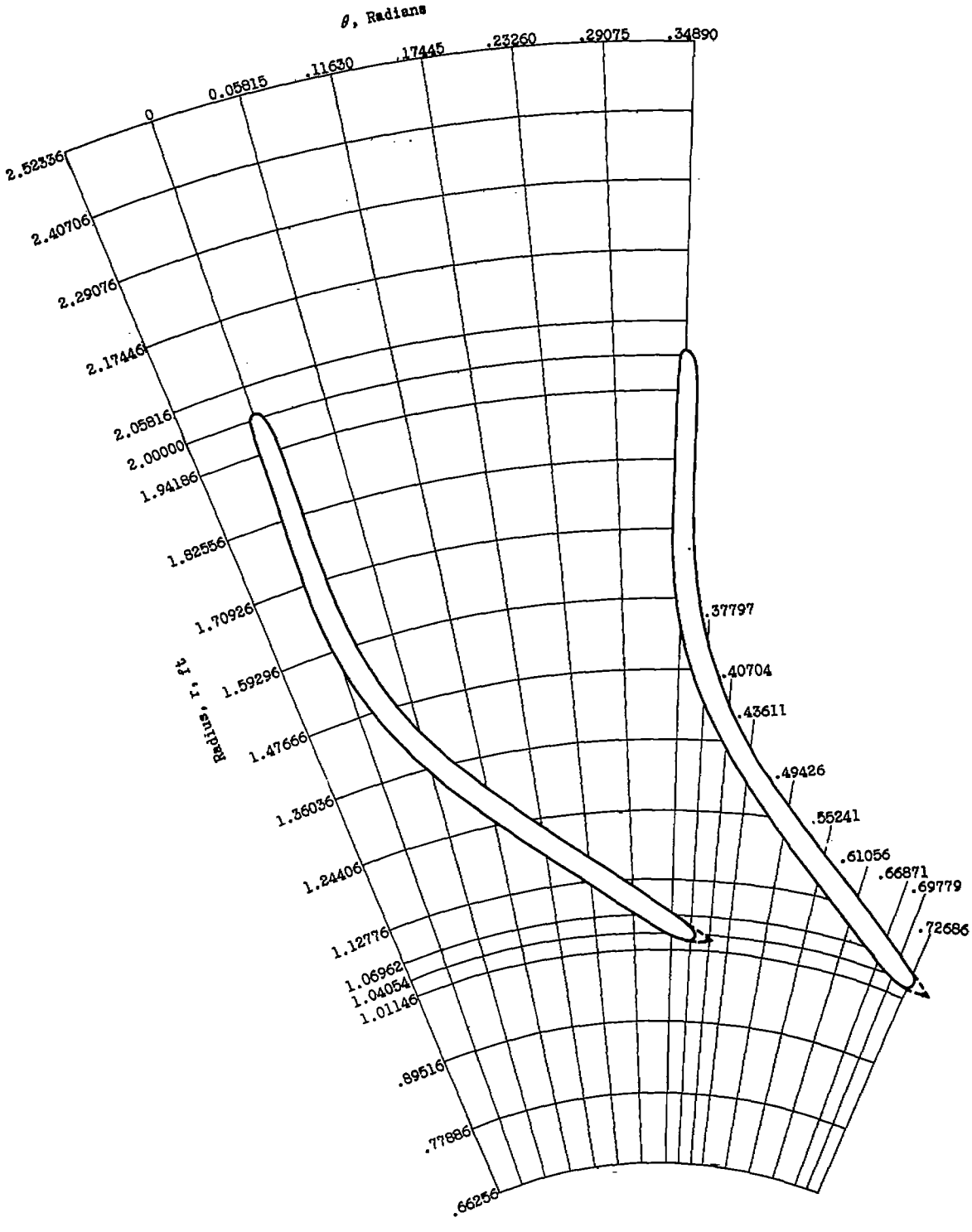

Figure 1. - Grid system for over-all solution.

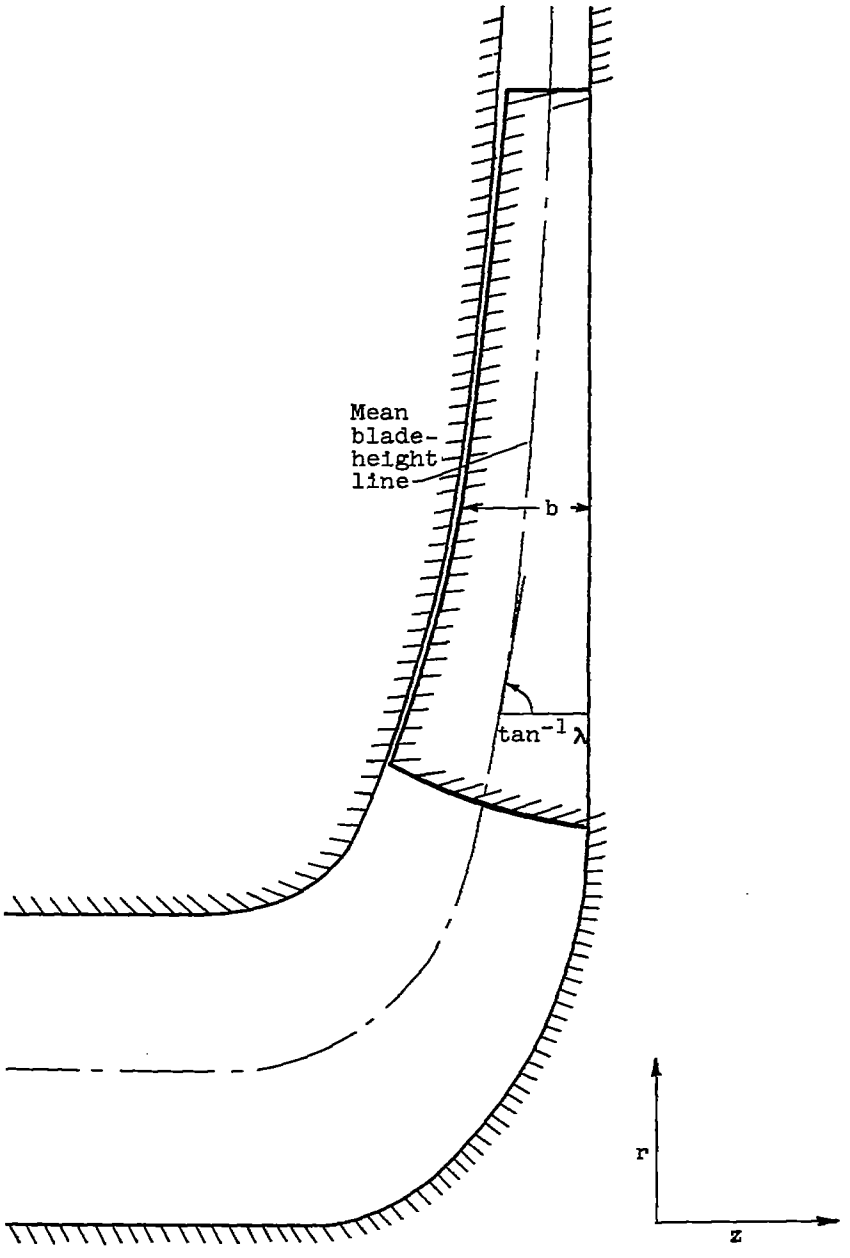

Figure 2. - Axial-radial plane view of 48-inch-diameter centrifugal impeller.

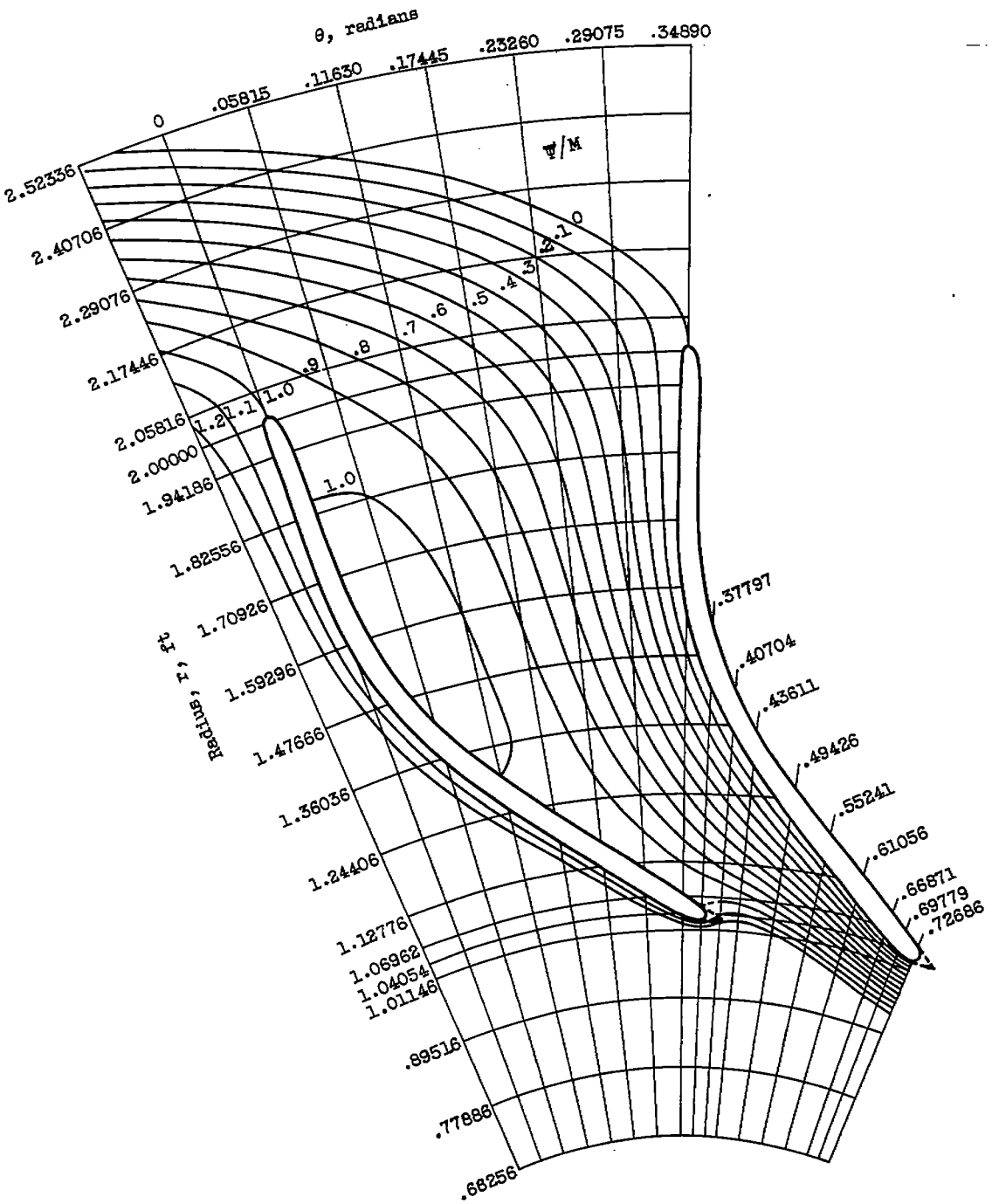

(a) Weight flow, 14 pounds per second (case A).

Figure 3. - Streamlines.

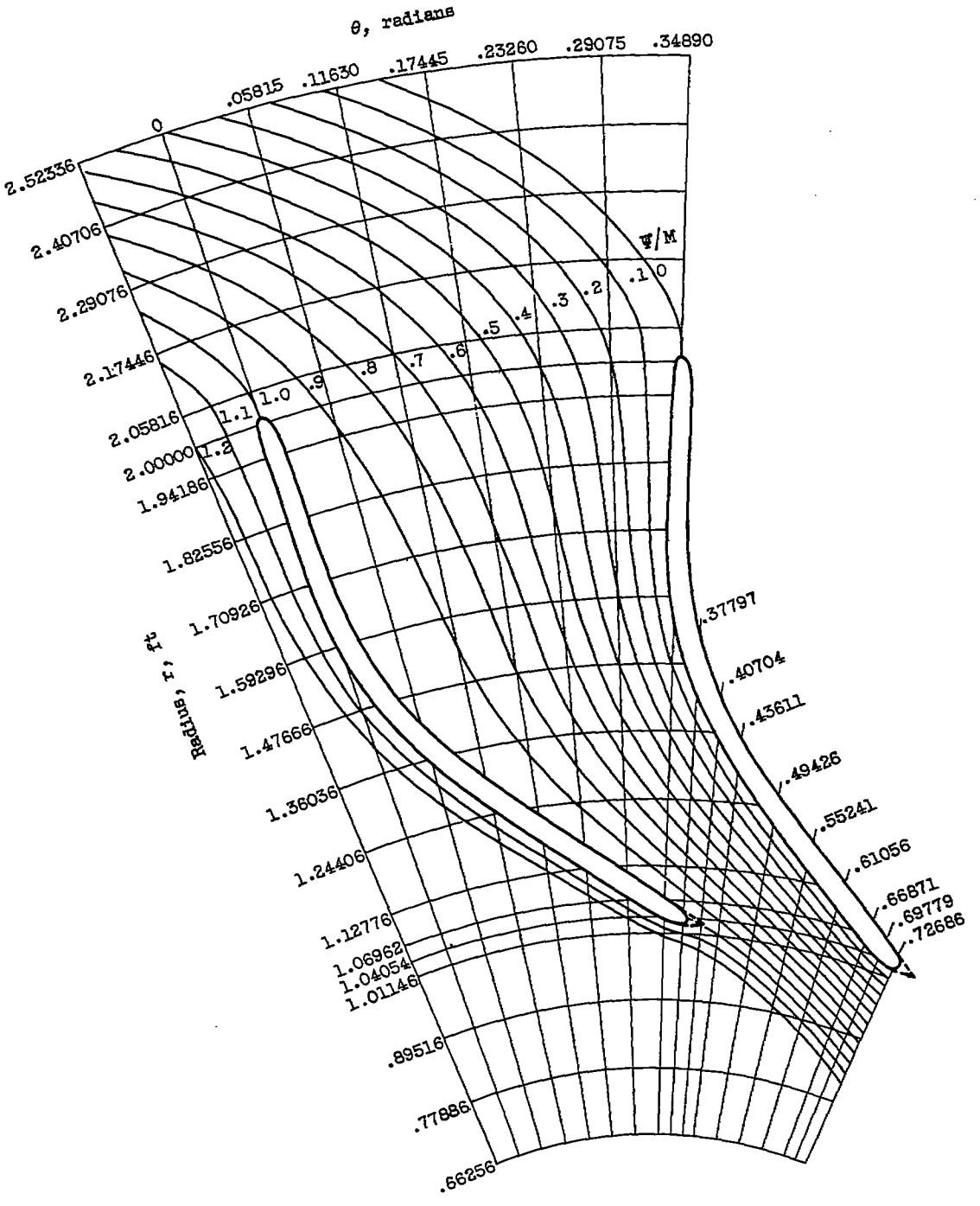

(b) Weight flow, 26.25 pounds per second (case B).

Figure 3. - Continued. Streamlines.

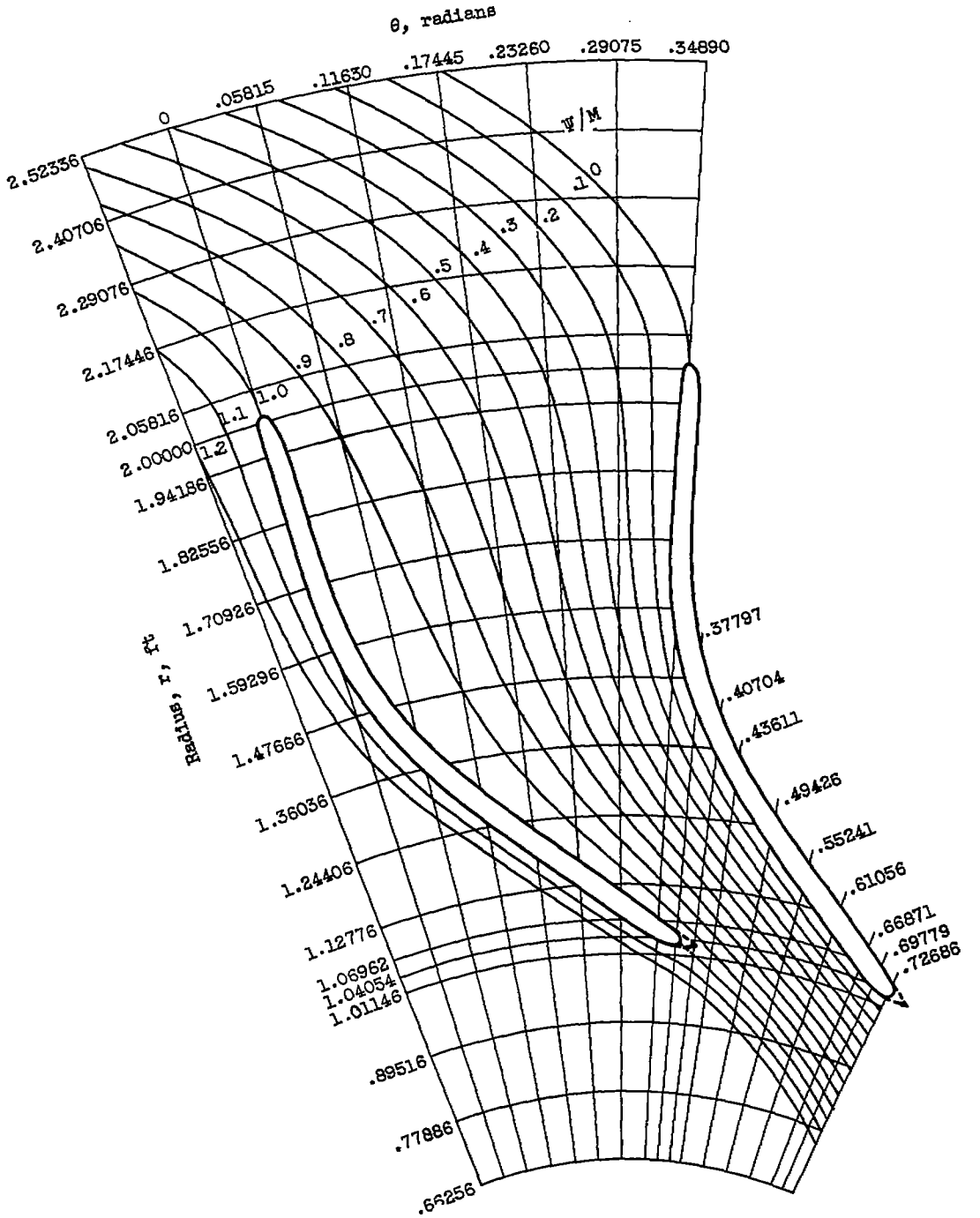

(c) Weight flow, 32.10 pounds per second (case C).

Figure 3. - Continued. Streamlines.

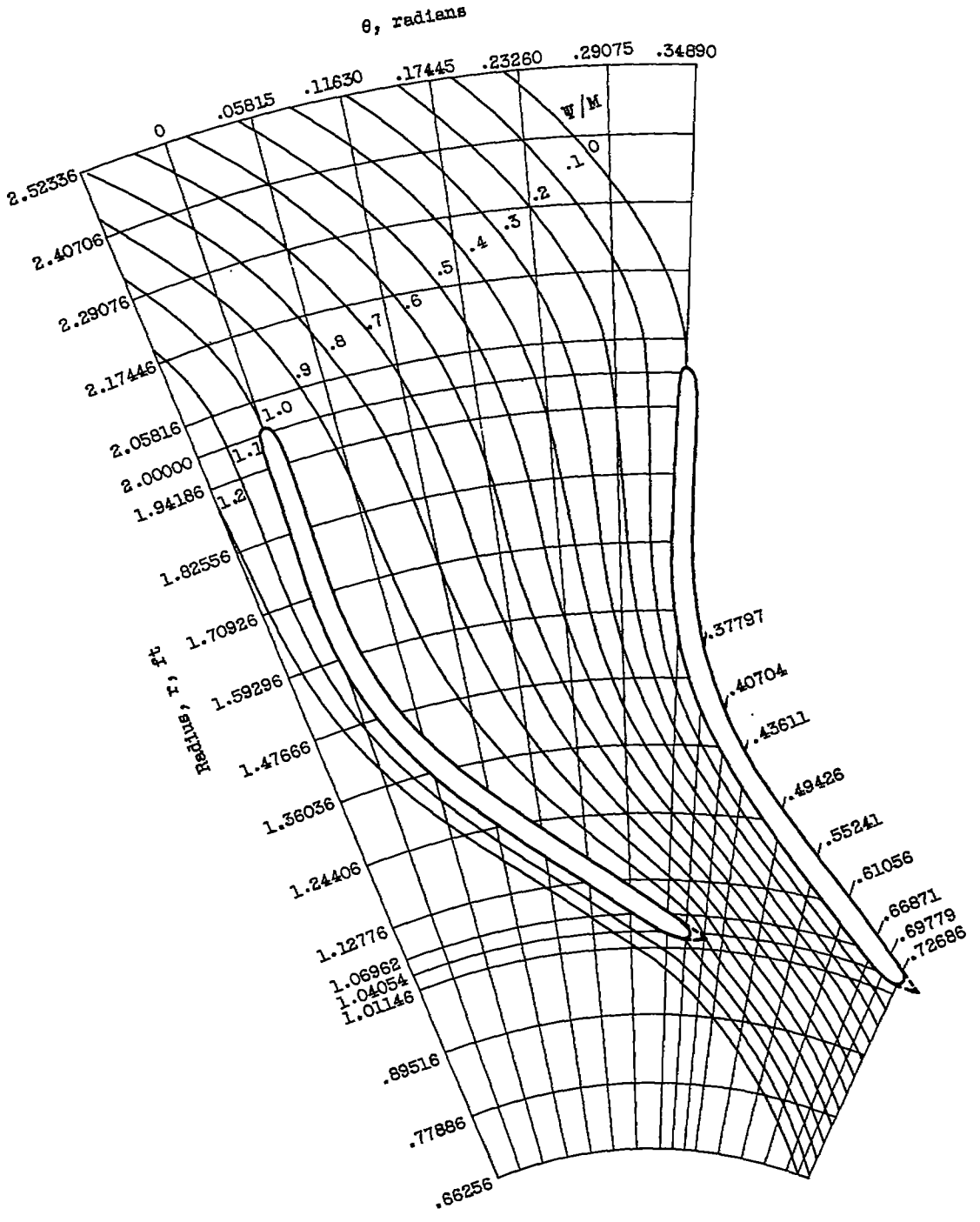

(d) Weight flow, 44 pounds per second (case D).

Figure 3. - Concluded. Streamlines.

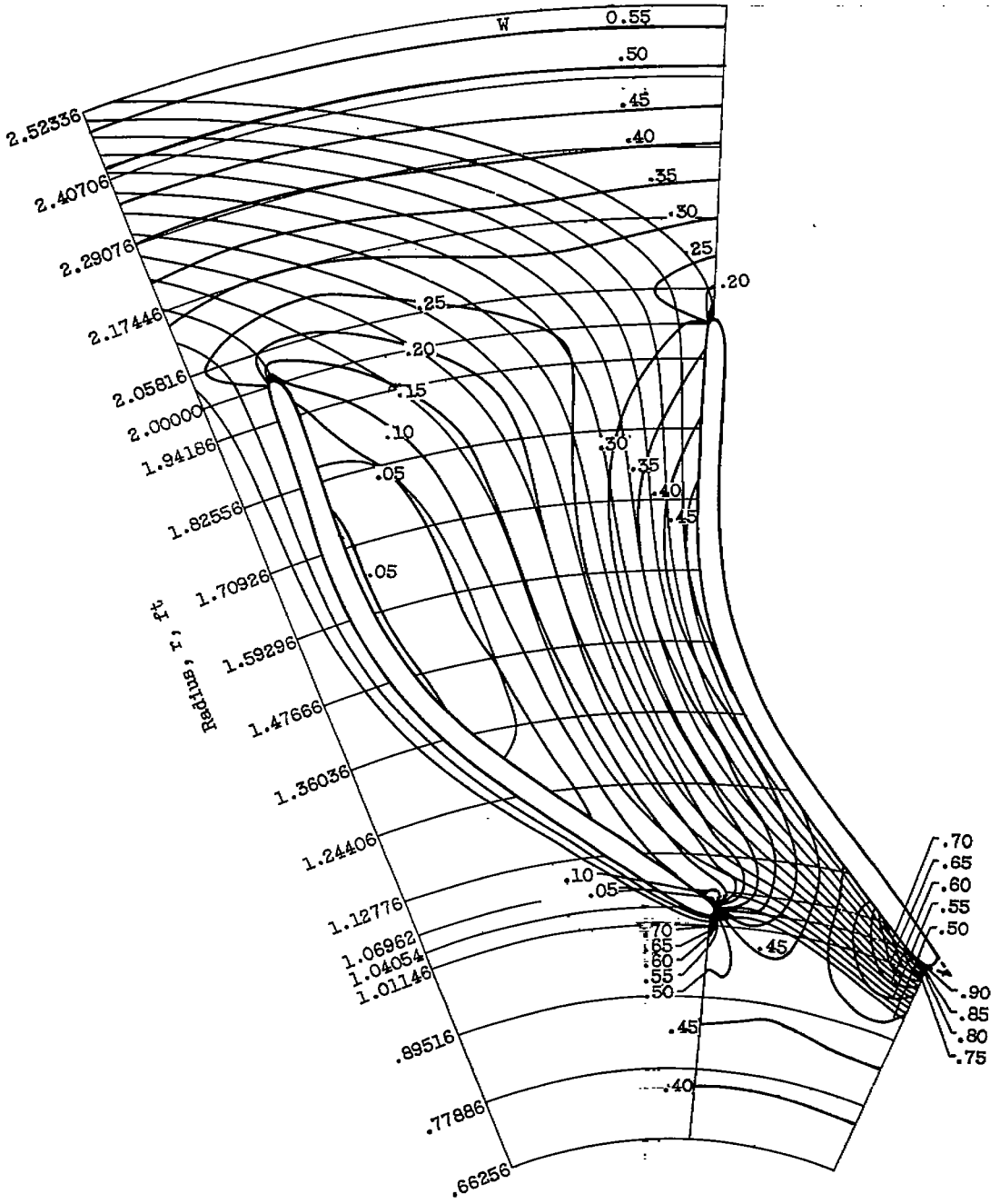

(a) Weight flow, 14 pounds per second (case A).

Figure 4. - Contours of constant relative velocity ratio W.

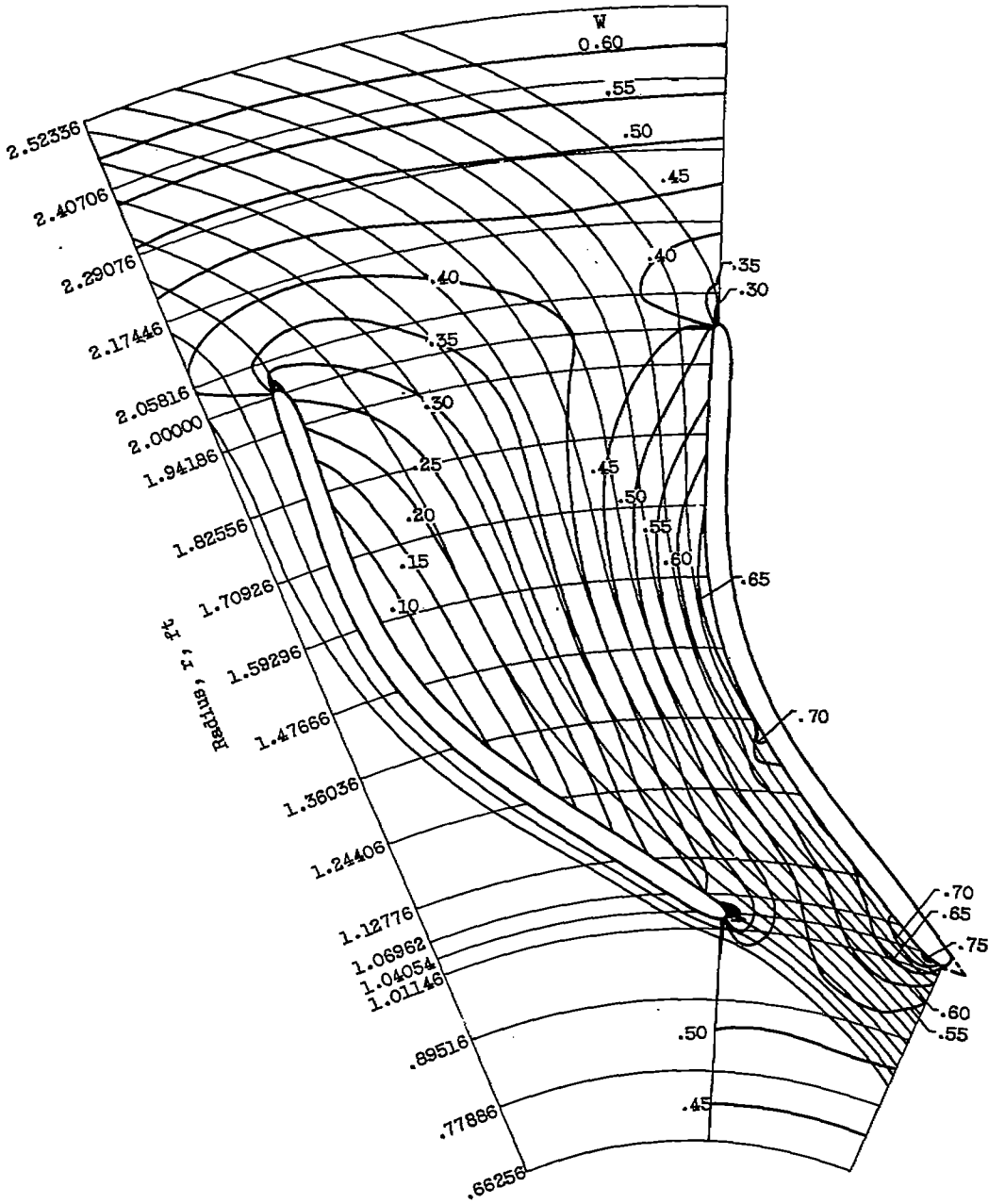

(b) Weight flow, 26.25 pounds per second (case B).

Figure 4. - Continued. Contours of constant relative velocity ratio W.

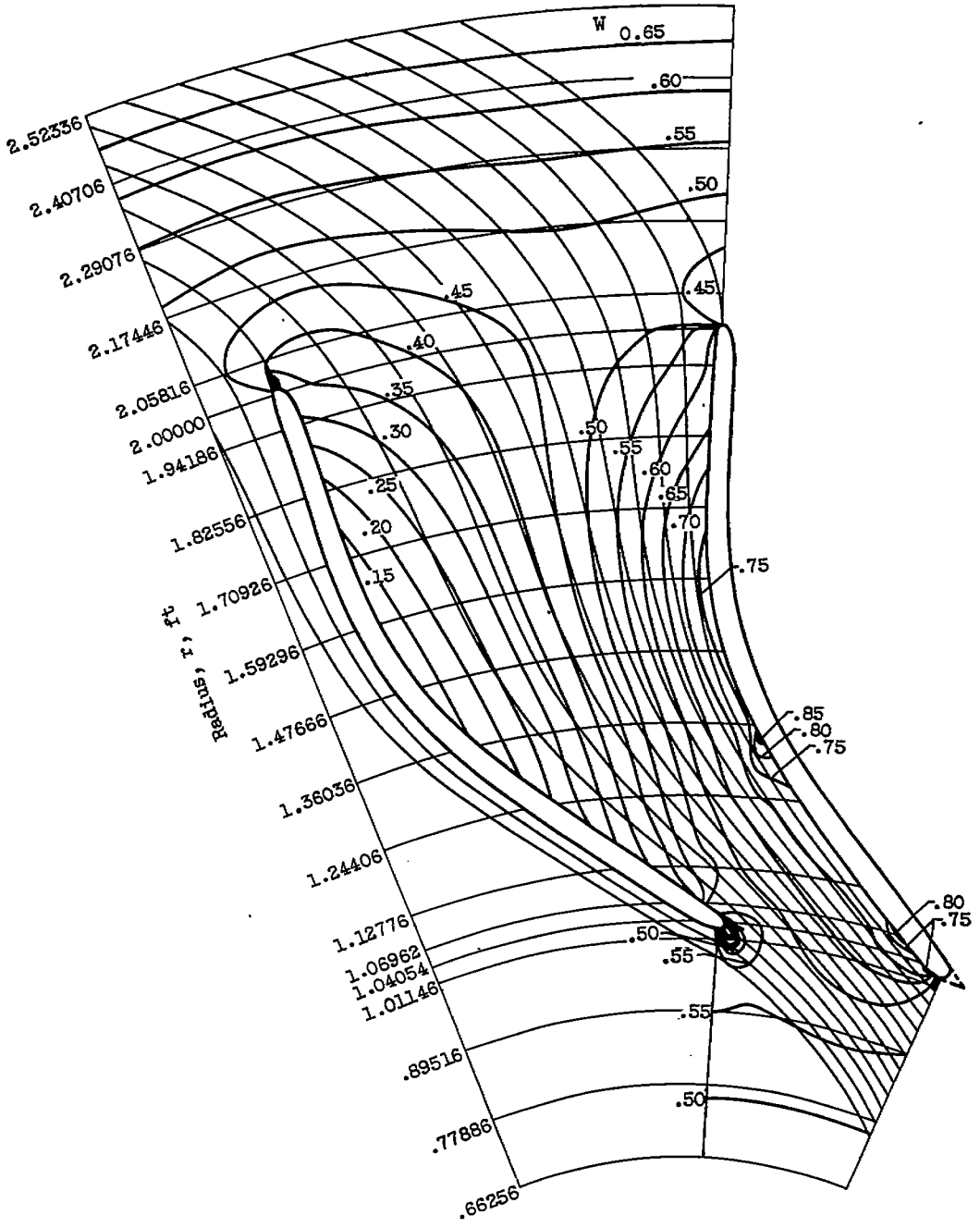

(c) Weight flow, 32.10 pounds per second (case C).

Figure 4. - Continued. Contours of constant relative velocity ratio W.

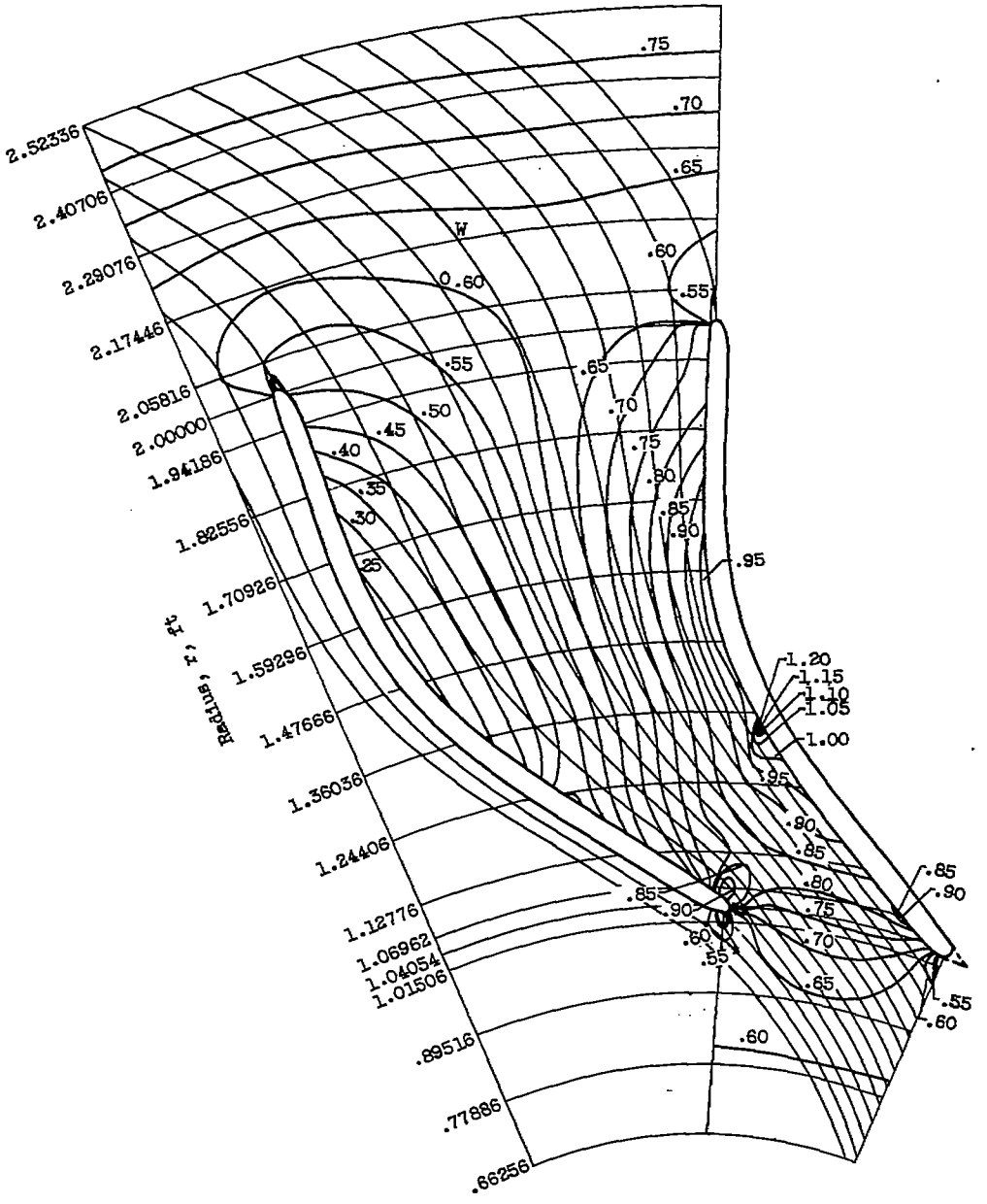

(d) Weight flow, 44 pounds per second (case D).

Figure 4. - Concluded. Contours of constant relative velocity ratio W.

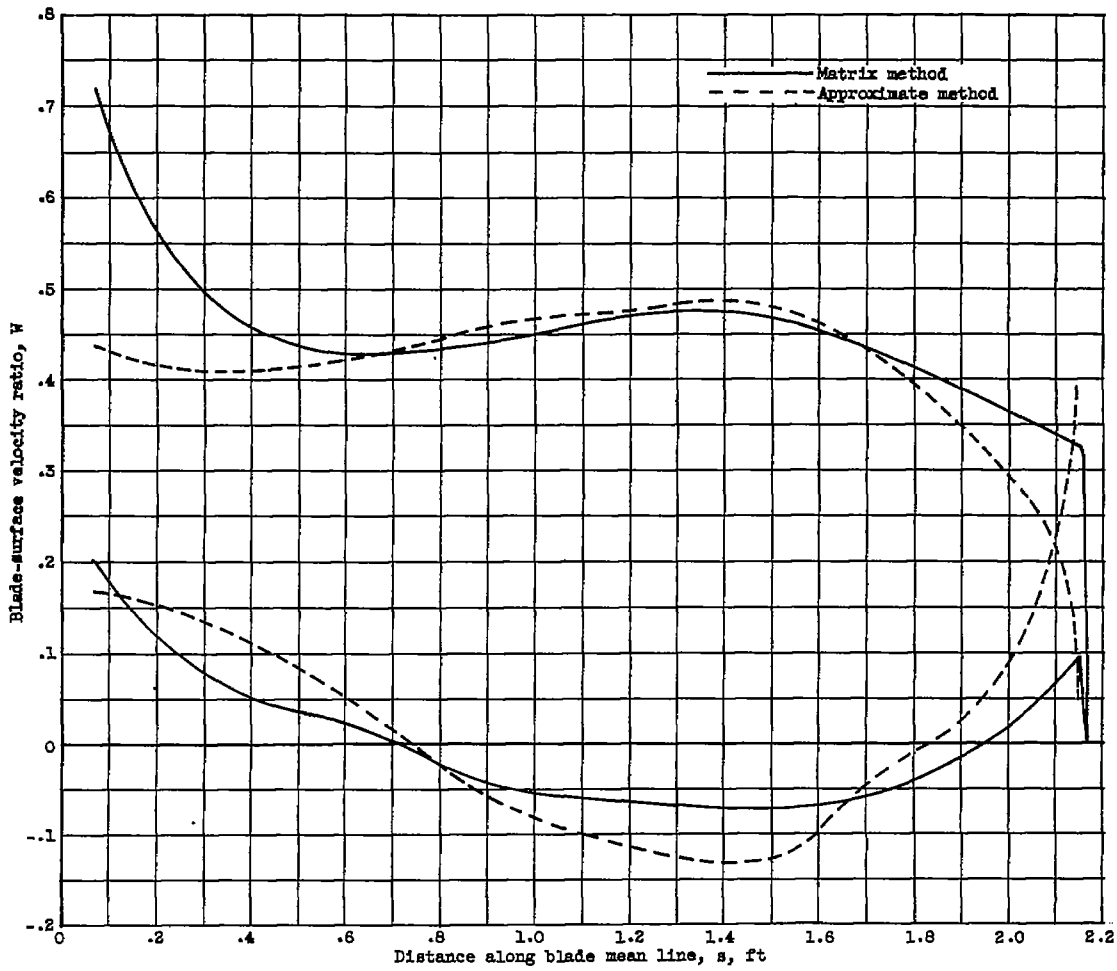

(a) Weight flow, 14 pounds per second (case A).

Figure 5. - Comparison of blade-surface velocity ratios obtained by approximate and matrix methods.

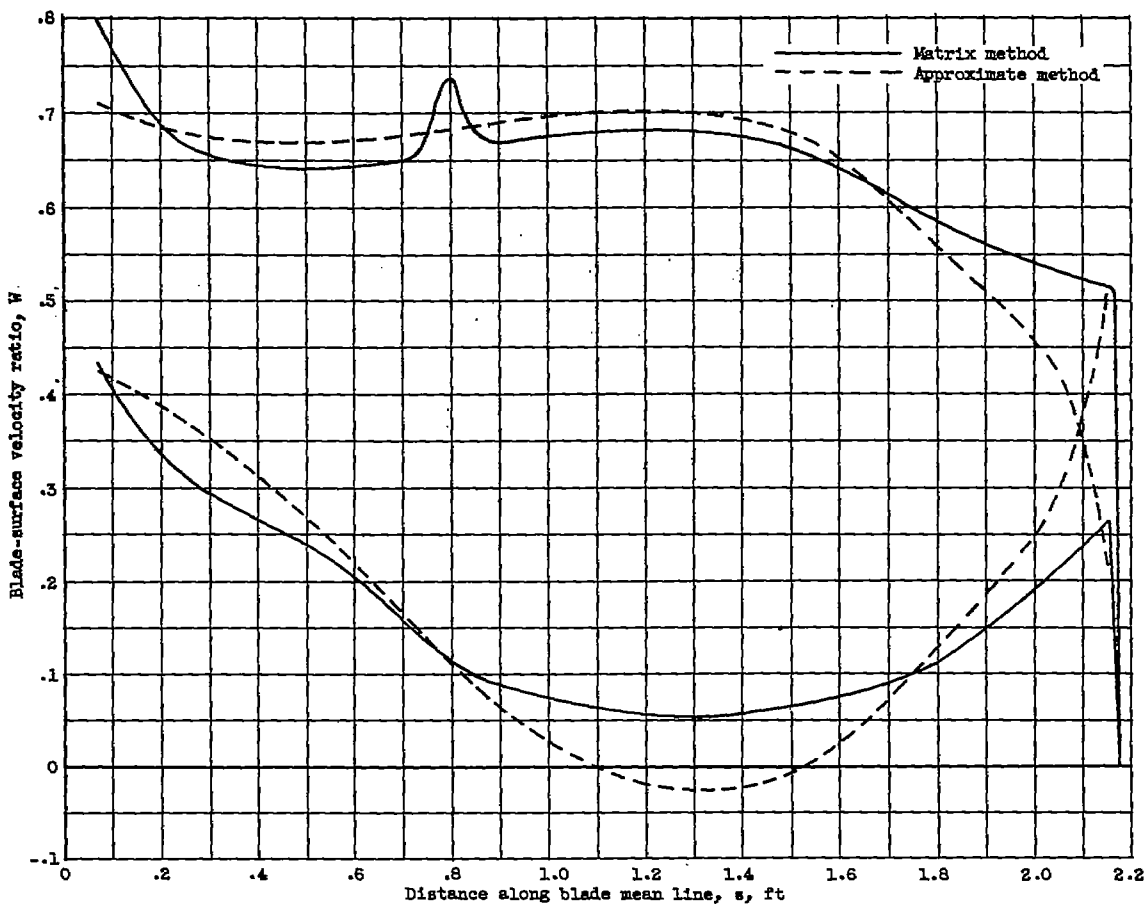

(b) Weight flow, 26.25 pounds per second (case B).

Figure 5. - Continued. Comparison of blade-surface velocity ratios obtained by approximate and matrix methods.

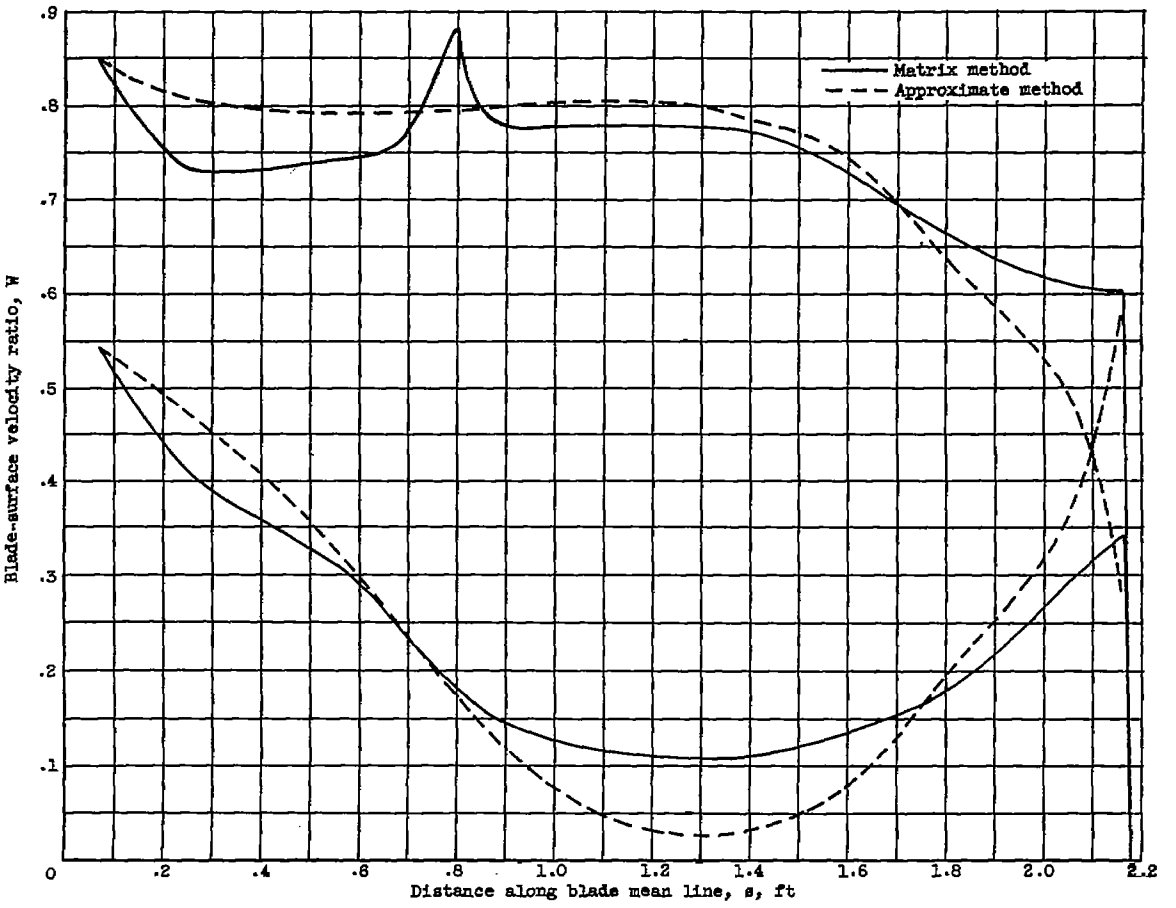

(c) Weight flow, 32.10 pounds per second (case C).

Figure 5. - Continued. Comparison of blade-surface velocity ratios obtained by approximate and matrix methods.

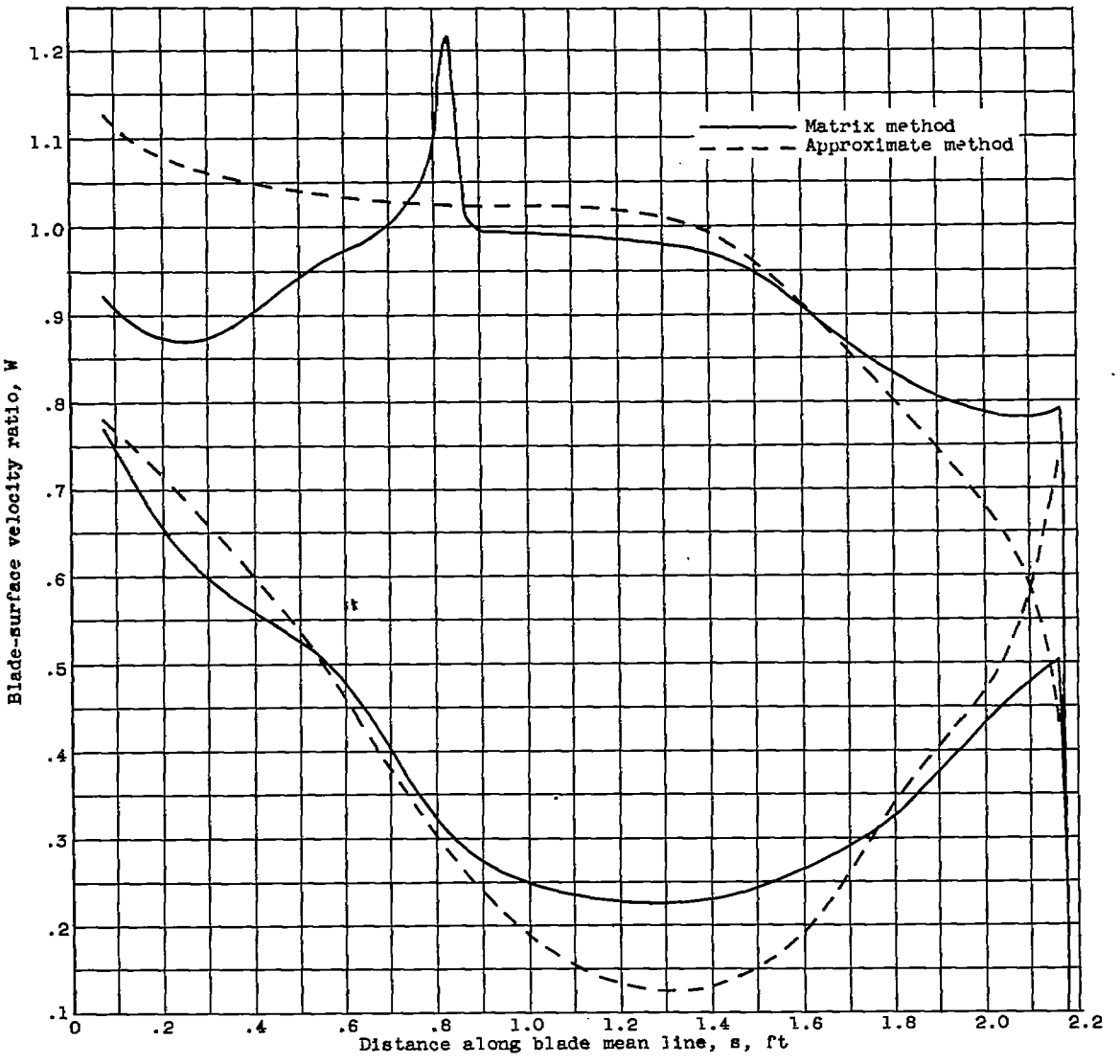

(d) Weight flow, 44 pounds per second (case D).

Figure 5. - Concluded. Comparison of blade-surface velocity ratios obtained by approximate and matrix methods.

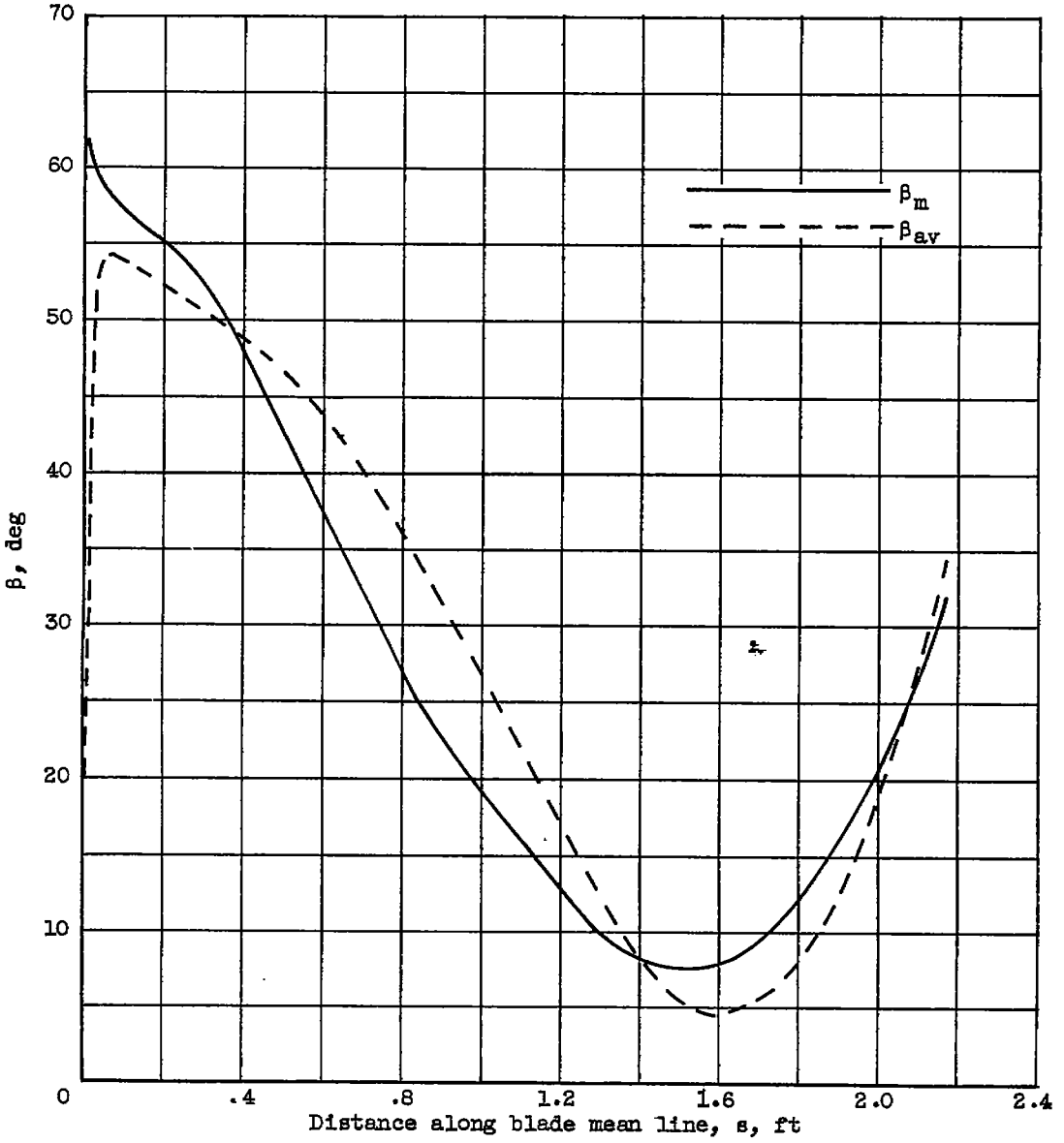

(a) Weight flow, 14 pounds per second (case A).

Figure 6. - Comparison of mass-averaged flow angle of exact solution β_m and approximation of β_m used in approximate method β_{av}.

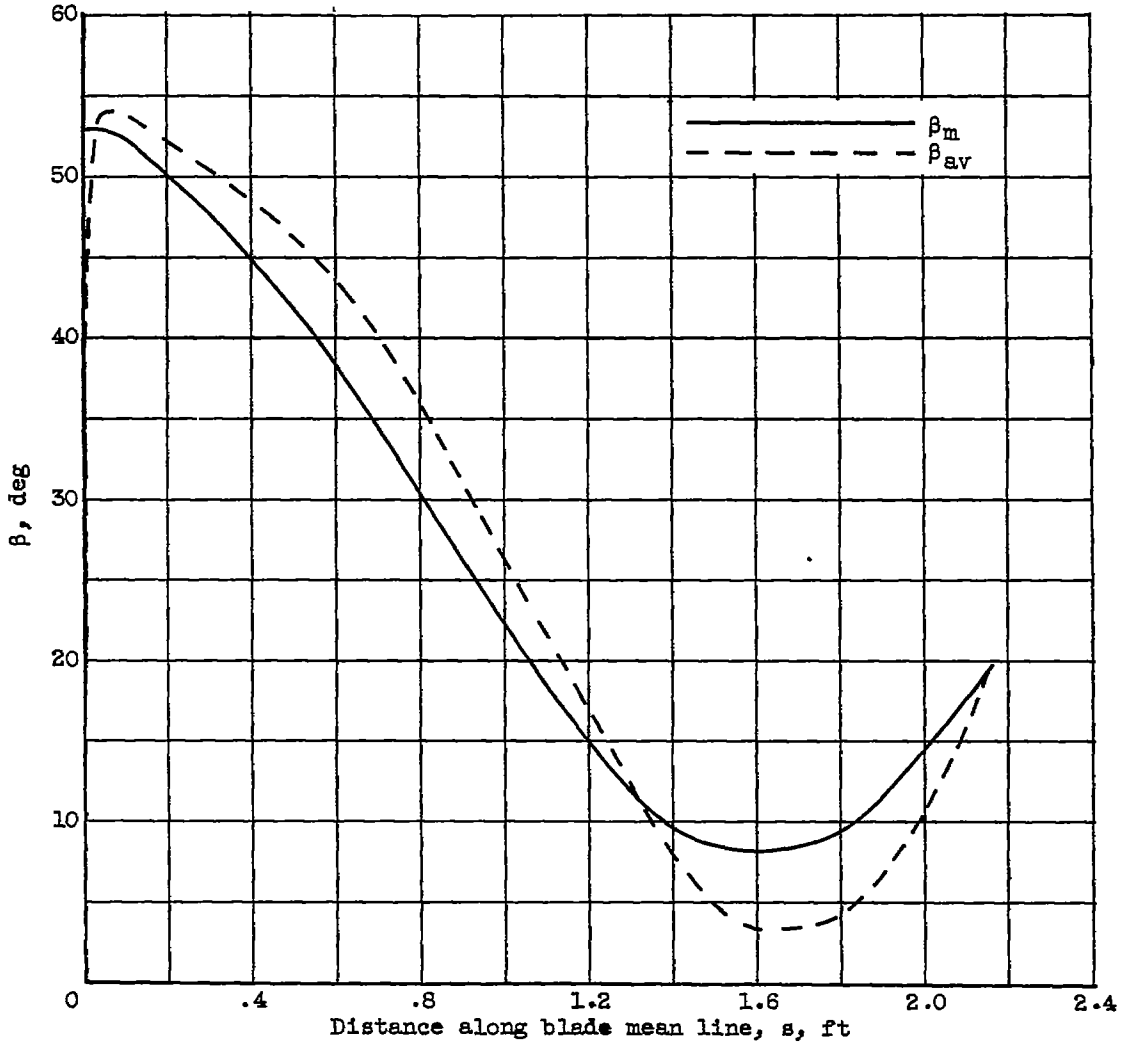

(b) Weight flow, 26.25 pounds per second (case B).

Figure 6. - Continued. Comparison of mass-averaged flow angle of exact solution β_m and approximation of β_m used in approximate method β_{av}.

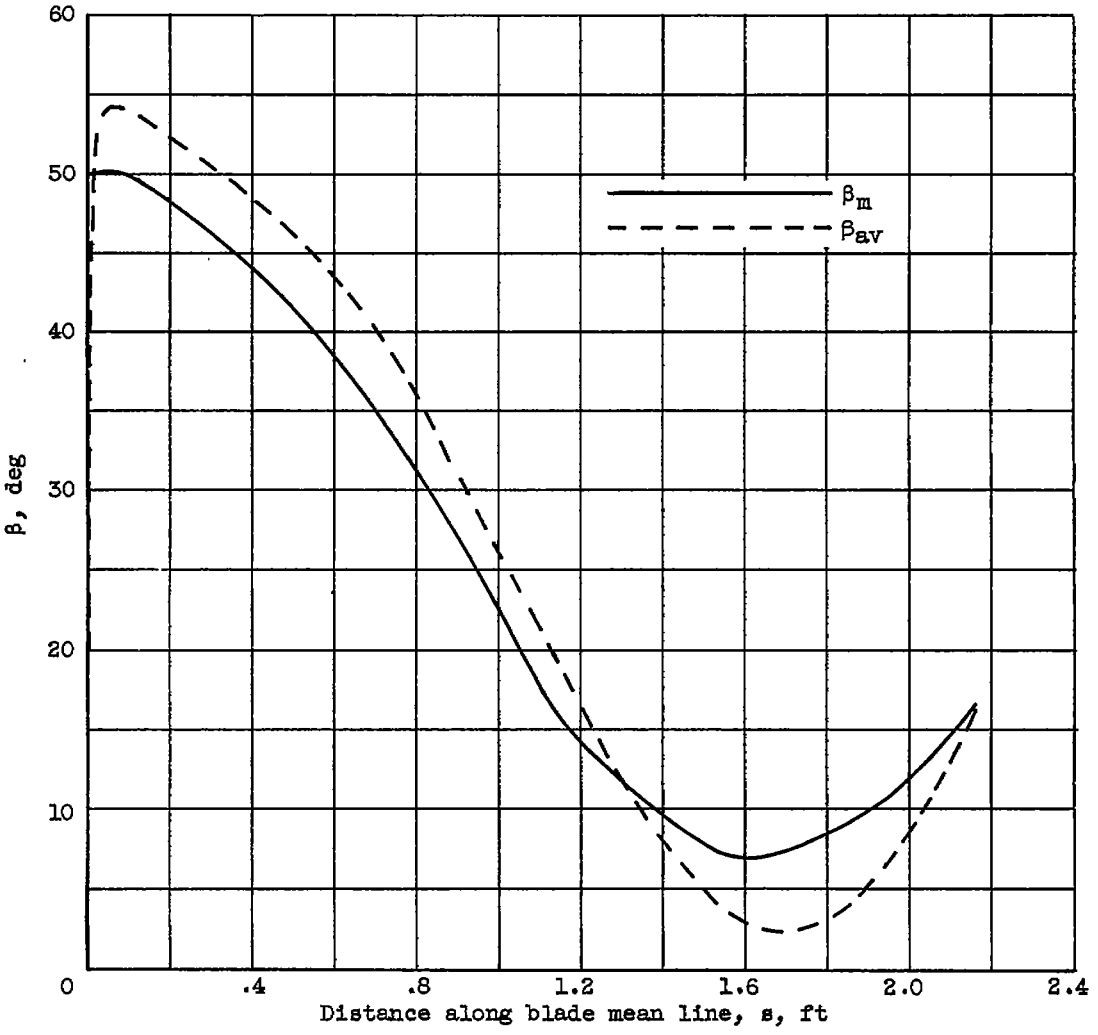

(c) Weight flow, 32.10 pounds per second (case C).

Figure 6. - Continued. Comparison of mass-averaged flow angle of exact solution β_m and approximation of β_m used in approximate method β_{av}.

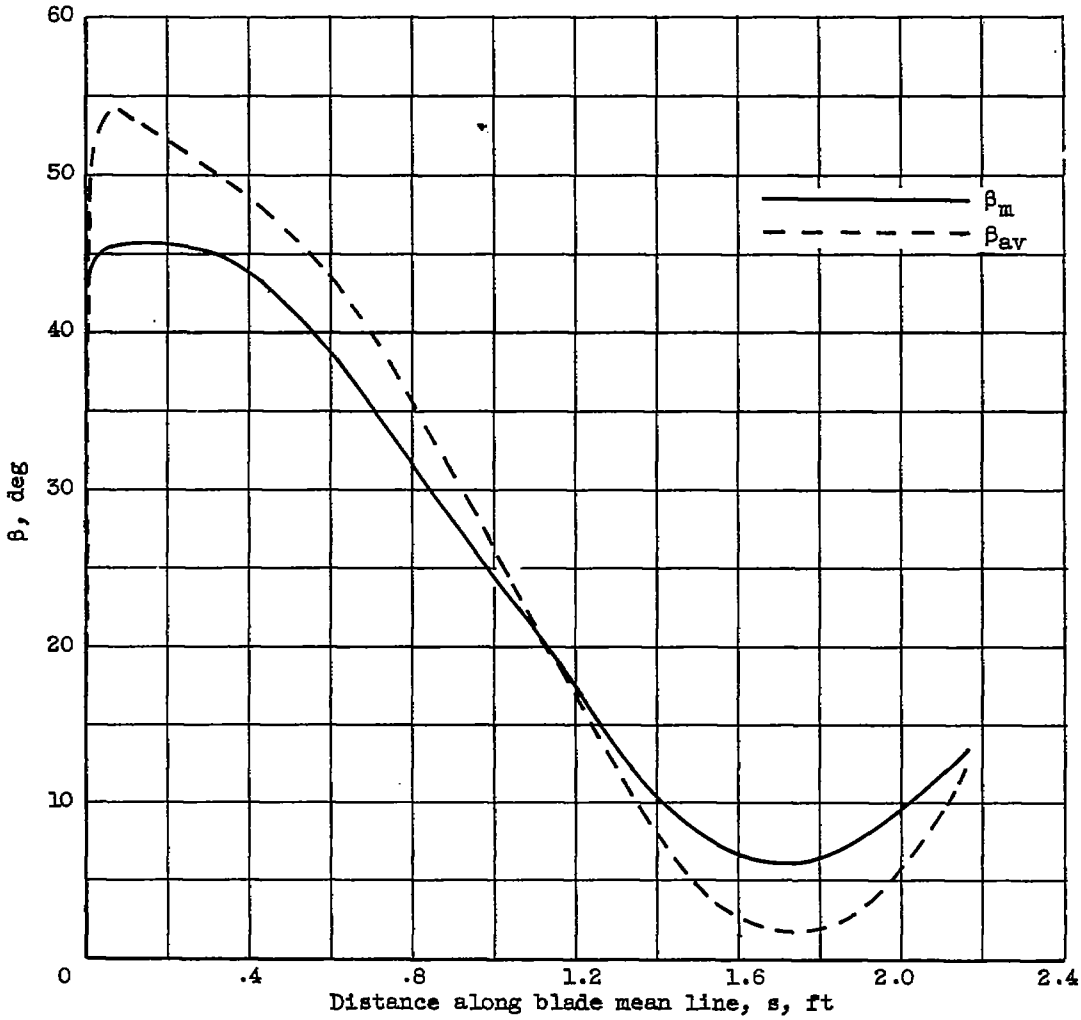

(d) Weight flow, 44 pounds per second (case D).

Figure 6. - Concluded. Comparison of mass-averaged flow angle of exact solution β_m and approximation of β_m used in approximate method β_{av}.

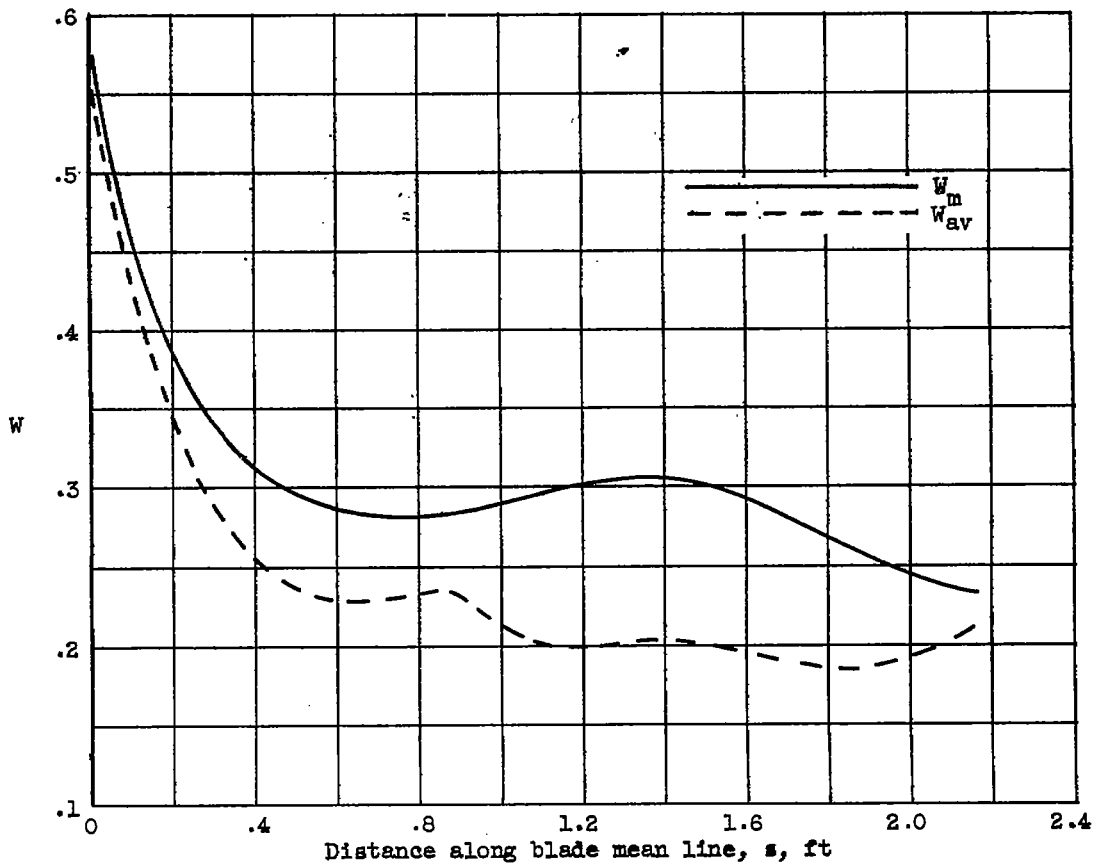

(a) Weight flow, 14 pounds per second (case A).

Figure 7. - Comparison of mass-averaged relative velocity ratio W_m with average of blade-surface velocity ratios W_{av}.

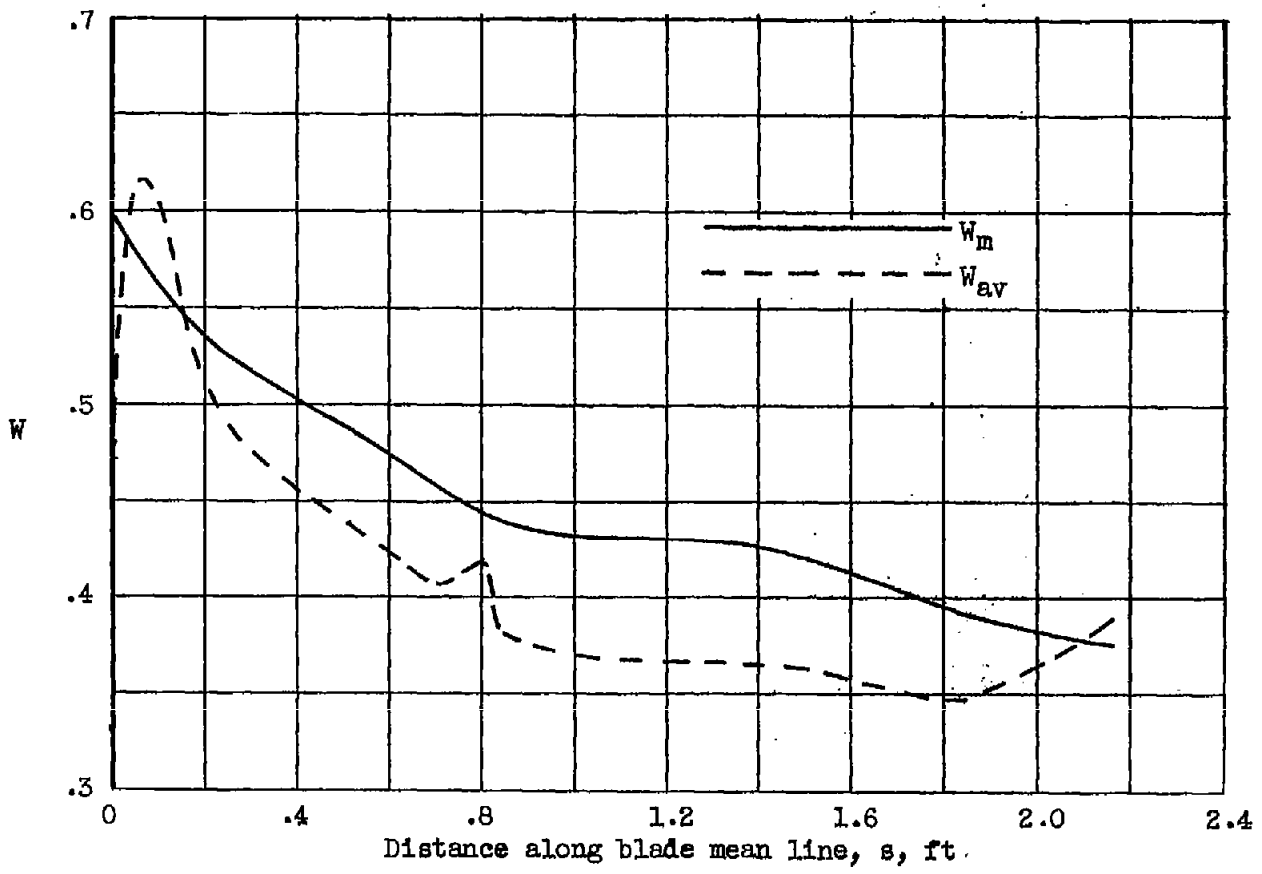

(b) Weight flow, 26.25 pounds per second (case B).

Figure 7. - Continued. Comparison of mass-averaged relative velocity ratio W_m with average of blade-surface velocity ratios W_{av}.

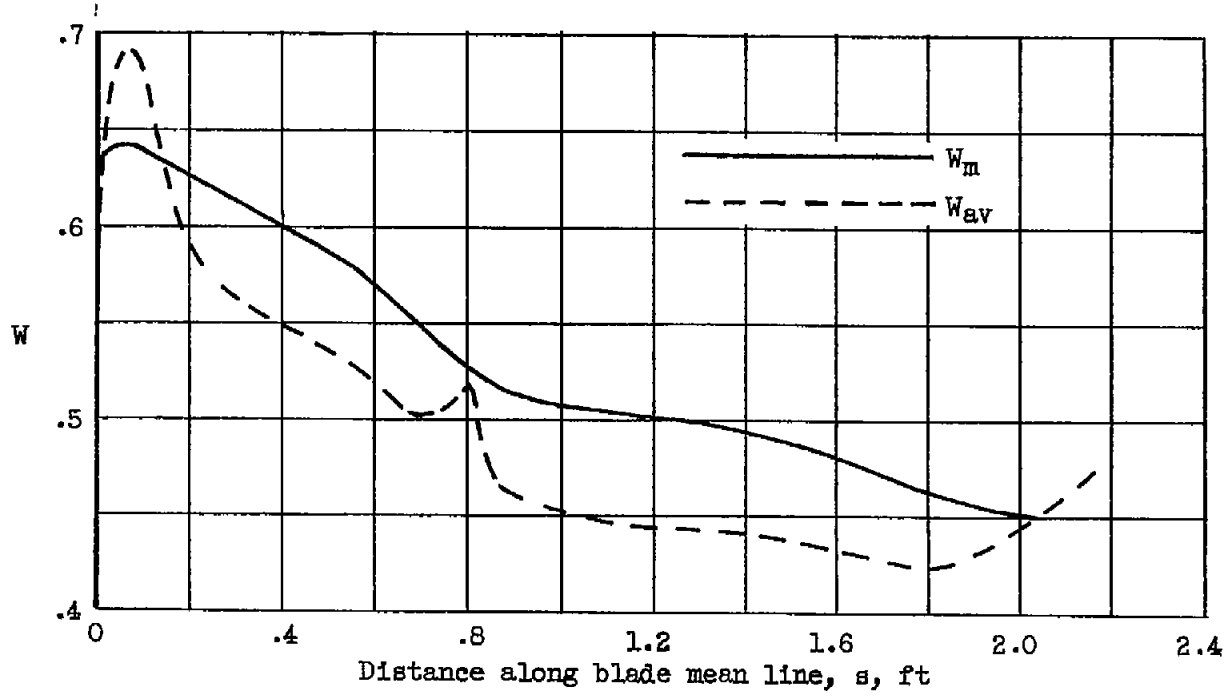

(c) Weight flow, 32.10 pounds per second (case C).

Figure 7. - Continued. Comparison of mass-averaged relative velocity ratio W_m with average of blade-surface velocity ratios W_{av}.

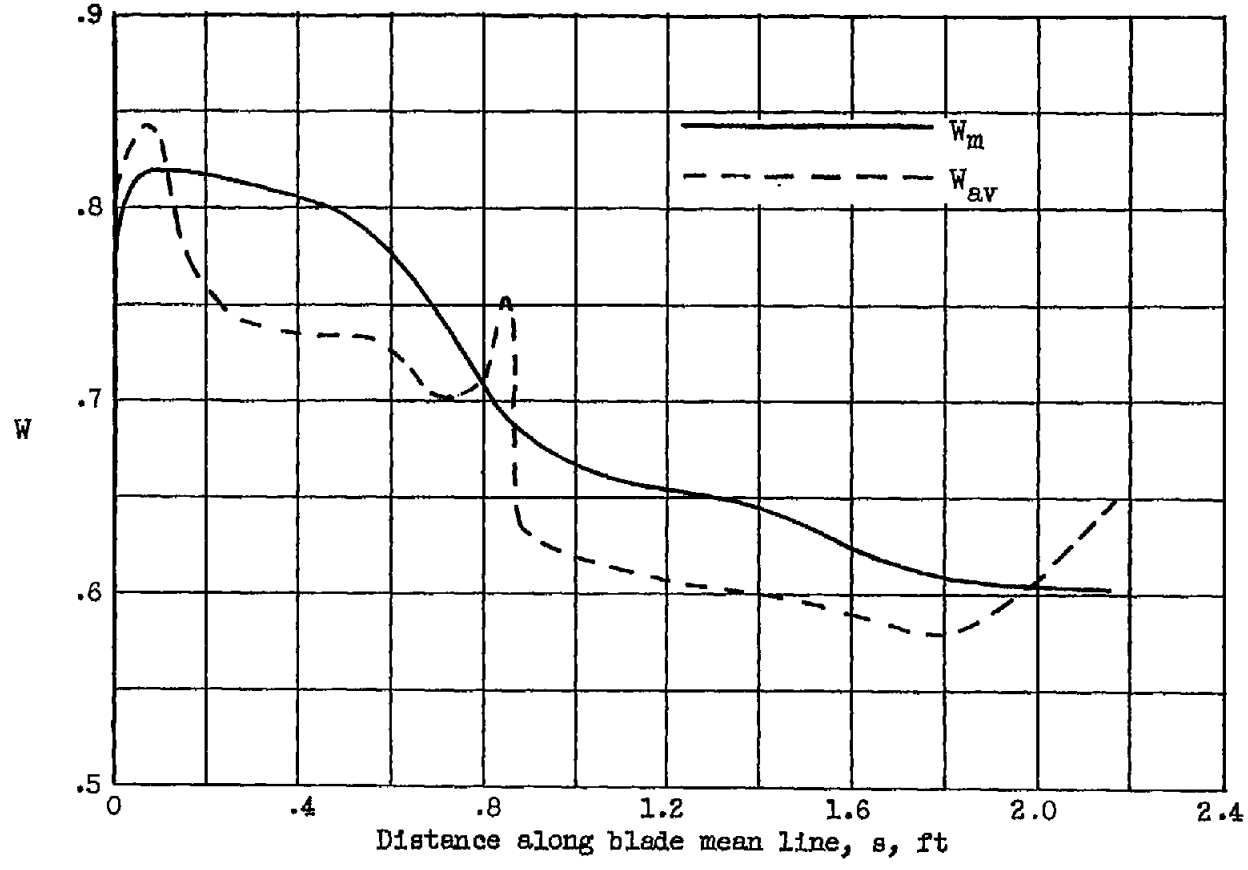

(d) Weight flow, 44 pounds per second (case D).

Figure 7. - Concluded. Comparison of mass-averaged relative velocity ratio W_m with average of blade-surface velocity ratios W_{av}.